RIGA TECHNICAL UNIVERSITY

Sandis Migla

DESIGN AND EXPERIMENTAL VALIDATION OF HIGH-RESOLUTION PULSE POSITION MODULATION TECHNIQUES FOR INTEGRATED SENSING AND COMMUNICATIONS

Summary of the Doctoral Thesis



RTU Press
Riga 2026

RIGA TECHNICAL UNIVERSITY
Faculty of Computer Science, Information Technology and Energy
Institute of Photonics, Electronics and Telecommunications

Sandis Migla
Doctoral Student of the Study Programme "Electronics"

DESIGN AND EXPERIMENTAL VALIDATION OF HIGH-RESOLUTION PULSE POSITION MODULATION TECHNIQUES FOR INTEGRATED SENSING AND COMMUNICATIONS

Summary of the Doctoral Thesis

Scientific supervisor

Professor Dr. sc. ing.
ARTŪRS ĀBOLTIŅŠ

RTU Press
Riga 2026

Migla, S. Design and Experimental Validation of High-Resolution Pulse Position Modulation Techniques for Integrated Sensing and Communications.
Summary of the Doctoral Thesis. – Riga: RTU Press, 2026. – 65 p.

Published in accordance with the decision of the Promotion Council "RTU P-08" of 14 September 2026, Minutes No. 56.







This research has been supported by the EU Recovery and Resilience Facility within the Project No. 5.2.1.1.i.0/2/24/I/CFLA/003, academic career doctoral grant (ID 1008), by the Latvian Council of Science grant No. lzp-2021/1-0475, "Picosecond-resolution pulse position modulation for beyond-the-limits energy efficiency of communications," and by the EU Cohesion Policy Fund Project No. 1.1.1.8/1/24/I/007 academic career doctoral grant (ID 8110).

Cover image from www.shutterstock.com.

https://doi.org/10.7250/9789934373718
ISBN 978-9934-37-371-8 (pdf)

DOCTORAL THESIS PROPOSED TO RIGA TECHNICAL UNIVERSITY
FOR PROMOTION TO THE SCIENTIFIC DEGREE
OF DOCTOR OF SCIENCE

To be granted the scientific degree of Doctor of Science (PhD), the present Doctoral Thesis has been submitted for defence at the open meeting of RTU Promotion Council on 18 December 2026, at 11:00, at the Faculty of Computer Science, Information Technology and Energy of Riga Technical University, 12 Āzenes Street, Room 201.

OFFICIAL REVIEWERS

Professor Dr. sc. ing. Jurģis Poriņš
Riga Technical University, Latvia

Professor Anna Baldycheva, PhD
University of Exeter, United Kingdom

Associate Professor Dr.phys. Jānis Alnis
University of Latvia, Latvia

DECLARATION OF ACADEMIC INTEGRITY

I hereby declare that the Doctoral Thesis submitted for review to Riga Technical University for promotion to the scientific degree of Doctor of Science (PhD) is my own. I confirm that this Doctoral Thesis has not been submitted to any other university for promotion to a scientific degree.

Sandis Migla _____

Date: _____

The Doctoral Thesis Summary has been written in English. It consists of Introduction, three chapters, Conclusions, References, 31 figures, and four tables; the total number of pages is 65. The Bibliography consists of 175 titles.

CONTENTS

INTRODUCTION 10
Rationale 10
Objective, Tasks, and Thesis to be Defended 12
Scientific Novelty and Main Results 13
The Approbation and Publications 14
The Structure of the Thesis 15
1 PPM SIGNAL GENERATION, DETECTION, AND MODULATOR PERFORMANCE EVALUATION 17
1.1 Pulse Position Modulation Types 17
1.2 PPM Signal Detection Methods 19
1.3 Digital Discovery-Based Testbed 20
1.4 Ultrashort Slot Duration Differential PPM 22
1.5 Digital Delay Line-Based PPM Modulator 23
1.6 Error Analysis and Correction Techniques 27
1.7 Summary of the First Thesis 30
2 ULTRASHORT PULSE EXPANSION IN PPM SYSTEMS 31
2.1 Electrical Pulse Expansion 31
2.2 Optical Pulse Expansion 34
2.3 Pulse Expansion Method Experimental Validation 35
2.4 Summary of the Second Thesis 37
3 EVALUATION OF PPM-BASED ISAC SYSTEM PERFORMANCE WITH AROF-BASED TRANSMISSION NETWORK 38
3.1 Design and Evaluation of 28 GHz Microwave/Optical Transmission System Utilizing PPM 38
3.2 Design and Evaluation of ISAC-Capable PPM-Based Radar System 41
3.3 Summary of the Third Thesis 47
CONCLUSIONS 48
REFERENCES 50

LIST OF FIGURES

1 Diagram of the Thesis structure, where “P” denotes the publications contained within the Thesis. 16
1.1 An example coherent PPM signal structure. 17
1.2 An example TR-PPM signal structure. 18
1.3 An example DPPM signal structure. ©2023 IEEE 19
1.4 Testbed software layer diagram. ©2022 IEEE 21
1.5 BER as a function of noise RMS for pulse durations 20 ns and 40 ns. ©2022 IEEE 21
1.6 Experimental setup for DPPM transmission including PEXM. ©2023 IEEE . . 22
1.7 Block diagram of the DDL-based modulator implementation. ©2024 IEEE . . 24
1.8 DPPM transmission test setup block diagram. ©2024 IEEE 24
1.9 Modulator jitter distribution measured by the ESTT. ©2024 IEEE 25
1.10 Experimental results for DPPM transmission tests. ©2024 IEEE 25
1.11 Conceptual block diagram of the PPM modulator. 26
1.12 Jitter distribution test results for the developed modulator: (a) jitter distribution; (b) pulse deviation from ideal positions. 27
1.13 Simulation results without clock drift error. ©2024 IEEE 29
1.14 Simulation results with added clock drift error. ©2024 IEEE 29
2.1 Pulse expanded using Mini-Circuits SLP-2400 filter: (a) waveforms of the pulses; (b) normalized magnitude spectra. 32
2.2 Custom-designed filters: (a) Magnitude-Normalized, and (b) Classical, with cutoff frequencies $f_c = 1.8$ GHz. 32
2.3 Ansys HFSS simulation results and custom-designed filter measurement results for group delay. 33
2.4 Pulse expanded using Classical custom-designed filter: (a) waveforms of the pulses; (b) normalized magnitude spectra. 33
2.5 Pulse expanded using Magnitude-Normalized custom-designed filter: (a) waveforms of the pulses; (b) normalized magnitude spectra. 33
2.6 Block diagram of optical pulse expansion test setup. 34
2.7 Pulse expanded using tunable FBG: (a) captured waveform, and (b) normalized magnitude spectra. 34
2.8 Block diagram of a PPM transmission link with an event timer for the demodulation. 35
2.9 BER versus average received optical power with optical pulse expansion with FBG module. 36
2.10 BER versus average received optical power with electrical pulse expansion with LPF. 37
3.1 Experimental setup of the PPM-based ARoF communication system. 39

3.2 Data transmission experiment results for the back-to-back (B2B) connection. . . 40
3.3 Data transmission experiment results for the connection with 20 km SMF. . . . 40
3.4 Setup block diagram of the ISAC-capable PPM-based radar system utilizing ARoF. 42
3.5 Measured BER as a function of slot duration: (a) without Gray coding, (b) with Gray coding. 45
3.6 Range measurement errorbar plot: (a) optical B2B connection, (b) optical connection with 40 km SMF, (c) optical connection with 40 km SMF and DCM. . 46

LIST OF TABLES

1.1 DPPM Transmission Experimental Parameters and Results ©2023 IEEE 23
2.1 TR-PPM Transmission Experiment Parameters 35
3.1 Summary of the Main Experimental Parameters 43
3.2 Range Measurement Results 46

ABBREVIATIONS

ADC analog-to-digital converter
ARoF analog radio-over-fiber
AWG arbitrary waveform generator
B2B back-to-back
BER bit error ratio
BPF bandpass filter
C-RAN centralized radio access network
CCSDS Consultative Committee for Space Data Systems
CD chromatic dispersion
CO central office
CS compressed sensing
CW continuous wave
D-MIMO distributed multiple-input multiple-output
DC direct current
DCM dispersion compensation module
DDL digital delay line
DPPM differential pulse position modulation
DSO digital storage oscilloscope
DTC digital-to-time converter
ECC error correcting code
ED envelope detector
EDFA erbium-doped fiber amplifier
ESA European Space Agency
ESTT Eventech Stream Time Tagger
FBG fiber Bragg grating
FEC forward error correction
FMCW frequency modulated continuous wave
FPGA field-programmable gate array
FSO free-space optical
FWHM full width at half maximum
IC integrated circuit
IoT Internet of Things
IR impulse radio
IR-UWB impulse radio ultra-wideband
ISAC integrated sensing and communications
LDPC low-density parity check
LPF low-pass filter

LVTTL low-voltage transistor–transistor logic
MZM Mach–Zehnder modulator
NASA National Aeronautics and Space Administration
NOE nonlinear optical effects
OOK on-off keying
PAM pulse amplitude modulation
PC personal computer
PCB printed circuit board
PD photodetector
PEXM pulse expansion module
PLC power line communication
PLL phase locked loop
PON passive optical network
PPM pulse position modulation
PRBS pseudorandom binary sequence
PWM pulse width modulation
RAU remote antenna unit
RF radio frequency
RMS root mean square
RoF radio-over-fiber
RS Reed–Solomon
SDK software development kit
SDR software-defined radio
SHF super-high-frequency
SLR satellite laser ranging
SMF single-mode optical fiber
SNR signal-to-noise ratio
SoC system-on-chip
TDC time-to-digital converter
ToA time of arrival
ToF time-of-flight
TR-PPM transmitted reference pulse position modulation
UAV unmanned aerial vehicle
UWB ultra-wideband
V2V vehicle-to-vehicle
V2X vehicle-to-everything
VOA variable optical attenuator
WGN white Gaussian noise
WPAN wireless personal area network

INTRODUCTION

Rationale

Energy efficiency is an essential aspect of a communication system, and it is crucial in applications with limited power budgets, i.e., space communications, sensor networks, and other autonomous systems using ultra-short pulses for transmitting information, as well as applications in integrated sensing and communications (ISAC), radar technology, and distributed sensor networks [1]. Ultra-wideband (UWB) technology provides an efficient means for creating power-efficient radio and optical communication systems. Well-known impulse radio ultra-wideband (IR-UWB) modulation schemes like IEEE 802.15.4a and its derivatives [2, 3] are designed for short-range wireless personal area networks (WPANs) and provide data rates of about 0.5 Mbit/s. There is numerous research for applying IR-UWB schemes and commercial devices for vehicle-to-vehicle (V2V) communications [4], railway [5], power line communication (PLC) [6], etc. However, due to limitations in achievable bitrate, impulse radio (IR) has not gained much popularity in high-speed terrestrial and space radio links, and most of the current research is concentrated on the employment of IR-UWB for localization and ranging [7]. However, with the introduction of 6G mobile networks, where it is predicted that ISAC will be one of the core functions of the radio network, excellent capabilities of IR-UWB for localization can facilitate the use of this technology also for communication [2].

Over the last decade, the amount of transmitted data and the data transmission speed have increased significantly. The urgency of the energy consumption associated with data transmission has increased correspondingly. Nowadays, communication systems designed to perform bandwidth-intensive high-speed data transmission extensively exploit microwave and optical frequency bands, thereby becoming increasingly demanding in energy consumption. With the transition to millimeter-wave carrier frequencies, power consumption plays an increasingly important role [8]. On the other hand, the availability of the spectrum at a millimeter band and the possibility of transmitting focused beams of optical or radio signals make UWB technology an attractive choice. Moreover, UWB signals allow for very accurate time-of-flight (ToF) measurements and precise localization, which is a feature in high demand.

To provide exceptional energy efficiency, the transmitted pulses must be as short as possible, and the only limitation is the communication channel's available bandwidth and the transceiver's capabilities. In radio communications, the bandwidth is determined by the radio frequency (RF) part and antenna. Nowadays, the bandwidth of the radio communication channel can reach hundreds of GHz. Therefore, pulses with a duration of a few picoseconds, theoretically, can be used. In the case of optical transmission, the length of the pulses can be below 1 ps.

Pulse position modulation (PPM) is UWB technology where information is encoded into the absolute or relative times of the signalling pulses [9–12], allowing ultra-short pulses to transmit data, increasing the power efficiency [13]. Because in PPM, the pulse duration does not carry

any information, average power and signal-to-noise ratio (SNR) of the transmitted signal do not directly affect the bit error ratio (BER). Instead, the instantaneous power of the signalling pulses plays a vital role in determining the communication system's performance. By shortening the signalling pulses, it is possible to decrease the average power and SNR without significant impact on BER [14]. Alternatively, it is possible to decrease BER, shortening the signalling pulses and increasing the instantaneous power. The benefits in both cases come at the expense of the frequency spectrum occupation. Therefore, there is no contradiction with the well-known Shannon formula for channel capacity.

PPM allows for substantial energy savings at the cost of spectrum occupation, which makes the proposed modulation technique of particular interest to users with limited energy resources and significant signal power losses in the communication channel, for example, deep space communications, terrestrial and underwater optical wireless sensor networks, etc. It might also be important for other users, since using the proposed modulation method can reduce overall energy consumption [15, 16].

While PPM was originally employed in analog low-frequency radio and microwave systems [17], it has subsequently found use in digital communications [18–20] and microwave applications. In the optical frequency range, PPM is used in free-space optical communication and wired communications [21–23]. Furthermore, PPM is still in use in semi-analog radio control systems [24].

An overview of the benefits, disadvantages, and applications of PPM can be found in [25]. The main advantage of PPM is that it ensures higher energy efficiency than other modulation techniques and is tolerant of nonlinear distortions [26–28]. Those properties provide a solid foundation for future use of PPM, as pointed out in [17, 29, 30]. The development of the PPM technique has led to novel hybrid modulation types, such as multi-pulse-position modulation [31], where the symbol is composed of several pulses. It is worth mentioning that PPM can be combined with pulse amplitude modulation (PAM) and pulse width modulation (PWM) techniques to increase the spectral efficiency of the transmission.

PPM is also used in space communications [32–37], and study [34] shows the implementation of a PPM modem capable of using a slot width as narrow as 0.5 ns for deep space communication experiment.

UWB modulation schemes [38, 39] are also used in optical communication systems using analog radio-over-fiber (ARoF) [40–42] and free-space optical (FSO) physical layers, allowing for competitive bitrates [43, 44] suitable for space communication, Internet of Things (IoT) applications, and underwater optical communications to be achieved [45]. Such communication systems widely employ the PPM technique [46–48].

The most significant challenges for transitioning to optical communication are providing high pointing accuracy and mitigating the atmospheric turbulence impact [49, 50]. The latest developments of optical ISAC for space and ground applications are highlighted in [51]. The employment of PPM in optical communication systems is especially appealing as optical circuitry

naturally operates at large frequency bandwidths, and optical fibers typically have very low signal attenuation. At the same time, traditional on-off keying (OOK) modulation techniques have higher optical power utilization and lower sensitivity to nonlinear distortions.

ISAC systems present a wide range of perspectives in the pursuit of launching 6G networks [52, 53] which promise to focus on more than just a communication-only standpoint, but to utilize existing infrastructure for novel applications, e.g., vehicle-to-everything (V2X) communication [54, 55], IoT [56], and unmanned aerial vehicle (UAV) surveillance [57]. ISAC has proven itself as a valuable method for enhancing energy and spectrum efficiency in IR-UWB systems and is used for range and Doppler shift sensing, as well as data transmission [58–60].

PPM is also one of the modulation formats used in ISAC applications, such as simultaneous communication and LiDAR [61, 62], or radar sensing based on chirp sequences [63], with its key advantages being high energy efficiency and resilience [64]. The study [65] shows a 45.2 % energy efficiency improvement compared to OOK.

Another application of PPM is in joint radar communication [63], which is explored in this Thesis. This PPM communication system with radar capabilities can work as an ISAC system, where the PPM transceiver's receiving antenna unit acts as a radar receiver. In this implementation, the transmitted signal can be locally used for symbol synchronization of the received waveform. Depending on the received reflections and pulses from other transmitters, distances and velocities of objects and receivers can be measured.

Objective, Tasks, and Theses to be Defended

The objective of the Thesis

Develop and experimentally validate a PPM-based ISAC-capable joint radar and communication system utilizing ARoF technology and a custom-built PPM modulator with a commercial time-tagger as the demodulator, which can serve as a testbed for future UWB sensing, as well as space communication research.

The defined tasks to achieve the objective

- Analyze and investigate the advantages and drawbacks of various PPM modulation schemes.
- Investigate and evaluate the use of a time-tagger for satellite laser ranging applications as a demodulator in PPM-based systems.
- Design, develop, and experimentally validate a digital delay line-based PPM modulator.
- Investigate error correction techniques in PPM-based systems.
- Investigate electrical and optical means of pulse expansion in systems utilizing a time tagger as the demodulator.
- Design, develop, and test a fiber optic-based PPM communication system.

- Develop and validate the concept of PPM-based integrated sensing and communications in a radar system.
- Investigate radio-over-fiber-based transmission of PPM signals.
- Investigate and evaluate the impact of various lengths of optical fiber in PPM data transmission and sensing systems.

Theses to be defended

1. A PPM modulator implemented using programmable gate and multiplexer-based digital delay line (DDL) integrated circuit (IC) technology is capable of achieving PPM pulse sequence generation with root mean square (RMS) timing jitter below 10 ps.
2. In time tagger-based PPM systems, a pulse with duration 50–100 ps can be expanded passively by electrical and optical means to more than 2 times its original full width at half maximum (FWHM) duration while preserving the pulse's waveform shape enough for stable detection.
3. In optical PPM-based ISAC systems, a BER below 1×10^{-6} along with a sensing accuracy below 5 cm at a range of at least 4 m with optical transmission distance exceeding 40 km can be achieved by using high-order PPM and a time tagger for satellite laser ranging (SLR) applications as the receiver.

Scientific Novelty and Main Results

The main scientific contributions of this Thesis

1. Experimentally demonstrated the concept of using digital delay line integrated circuits for high-order high-precision PPM pulse sequence generation.
2. Experimentally proved the concept of using a high-precision time tagger for satellite laser ranging applications to achieve high-order PPM signal demodulation.
3. Experimentally proven electrical and optical pulse stretching techniques for use in PPM communication systems.
4. For the first time experimentally demonstrated joint radar sensing and communications using PPM in a system employing analog radio-over-fiber technology with long fiber spans.

The main results of the presented Thesis have been utilized in three research projects

1. EU Recovery and Resilience Facility Project No. 5.2.1.1.i.0/2/24/I/CFLA/003 academic career doctoral grant (ID 1008).
2. Latvian Council of Science grant No. lzp-2021/1-0475, "Picosecond-resolution pulse position modulation for beyond-the-limits energy efficiency of communications."
3. EU Cohesion Policy Fund Project No. 1.1.1.8/1/24/I/007 academic career doctoral grant (ID 8110).

The Approbation and Publications

The main results presented in this Thesis have been published in three peer-reviewed international journals ranking in the top 25th percentile (Q1) by citation index, as well as four peer-reviewed international conference proceedings.

Dissemination in international conferences

1. 2022 IEEE 2nd Ukrainian Microwave Week (UkrMW), November 14–18, 2022, Kharkiv, Ukraine.
2. 2023 IEEE 10th Jubilee Workshop on Advances in Information, Electronic and Electrical Engineering (AIEEE), April 27–29, 2023, Vilnius, Lithuania.
3. 2024 Joint European Conference on Networks and Communications & 6G Summit (EuCNC/6G Summit), June 3–6, 2024, Antwerp, Belgium.
4. 2024 IEEE International Conference on Microwaves, Communications, Antennas, Biomedical Engineering and Electronic Systems (COMCAS), July 9–11, 2024, Tel Aviv, Israel.

Publications in conference proceedings

[66] Migla, S., Selis, O., Sics, P. E., Pudzs, M., Zeltins, M., and Aboltins, A. "A Design of UWB Communication Testbed with Event Timer-based PPM Demodulator." *2022 IEEE 2nd Ukrainian Microwave Week (UkrMW)*. 2022, pp. 691–694. DOI: 10.1109/UkrMW58013.2022.10037100

[67] Selis, O., Migla, S., Sics, P. E., Zeltins, M., Spolitis, S., and Aboltins, A. "Demonstration of 50 ps Per-Position Differential Pulse Position Modulation Data Transmission." *2023 IEEE 10th Jubilee Workshop on Advances in Information, Electronic and Electrical Engineering (AIEEE)*. 2023, pp. 1–4. DOI: 10.1109/AIEEE58915.2023.10134802

[68] Sics, P. E., Tihomorskis, N., Migla, S., Ratners, J., Kurtenoks, V., and Aboltins, A. "Implementation of Reconfigurable 149Mbps TDC-Based PPM Transceiver." *2024 Joint European Conference on Networks and Communications & 6G Summit (EuCNC/6G Summit)*. 2024, pp. 706–710. DOI: 10.1109/EuCNC/6GSummit60053.2024.10597124

[69] Migla, S., Selis, O., Sics, P. E., and Aboltins, A. "Error Analysis and Correction Techniques for PPM Communication Links with Jitter and Clock Drift." *2024 IEEE International Conference on Microwaves, Communications, Antennas, Biomedical Engineering and Electronic Systems (COMCAS)*. 2024, pp. 1–4. DOI: 10.1109/COMCAS58210.2024.10666259

Publications in scientific journals

[70] Aboltins, A., Solovjova, T., Semenako, J., Kusnins, R., Migla, S., Sics, P. E., Selis, O., Tihomorskis, N., Prigunovs, D., Ostrovskis, A., and Spolitis, S. "Passive Electrical and Optical Methods of Ultra-Short Pulse Expansion for Event Timer-Based TDC in PPM Receiver." *Electronics* 12.22 (2023). DOI: 10.3390/electronics12224634

[71] Migla, S., Rubuls, K., Tihomorskis, N., Salgals, T., Ozolins, O., Bobrovs, V., Spolitis, S., and Aboltins, A. "Ultra-Wideband Analog Radio-over-Fiber Communication System Employing Pulse-Position Modulation." *Applied Sciences* 15.8 (2025). DOI: 10.3390/app15084222

[72] Migla, S., Tihomorskis, N., Rubuls, K., Cirjulina, D., Murans, I., Kurtenoks, V., Braunfelds, J., Spolitis, S., Ozolins, O., Vovchuk, D., Salgals, T., Ginzburg, P., Bobrovs, V., and Aboltins, A. "Demonstration of Integrated Sensing and Communications in an ARoF-Based Radar System Utilizing Pulse Position Modulation." *IEEE Access* 14 (2026), pp. 76251–76264. DOI: 10.1109/ACCESS.2026.3693952

The Structure of the Thesis

The Thesis is written as a summary of thematically unified scientific publications. Each chapter is devoted to its corresponding thesis.

Chapter 1 introduces the used PPM types and detection methods. A Digital Discovery-based testbed is presented, which serves as the first stepping stone in this research. This chapter introduces the concept of using a commercial time-tagger (also known as an event timer) for SLR applications as a PPM demodulator. The main focus point of this chapter is the design and performance evaluation of a digital delay line integrated circuit-based PPM modulator. The chapter is concluded with systematic error and jitter mitigation techniques in PPM communication systems.

Chapter 2 is devoted to the electrical and optical pulse expansion techniques in PPM communication systems. Custom-built filter-based and an fiber Bragg grating (FBG)-based optical pulse expansion setups are presented. This chapter is concluded with the experimental evaluation of both methods in a fiber optic-based PPM communication system by transmitting pseudorandom binary sequence (PRBS).

Chapter 3 introduces ARoF as a viable method for RF-modulated PPM signal transmission over long distances. An experimental setup for ARoF-based communication system using PPM is presented. The chapter is concluded with an experimental demonstration of ISAC using PPM in an ARoF-based radar system, presenting BER measurements and sensing distance accuracy measurements.

Finally, the Thesis is concluded by summarizing the main findings presented in the men-

tioned chapters, conclusions drawn about each thesis to be proved, and discussing future prospects of UWB-based ISAC research.

The overview of publications contained within this Thesis and their relationships with chapters and research objectives is shown in Fig. 1.

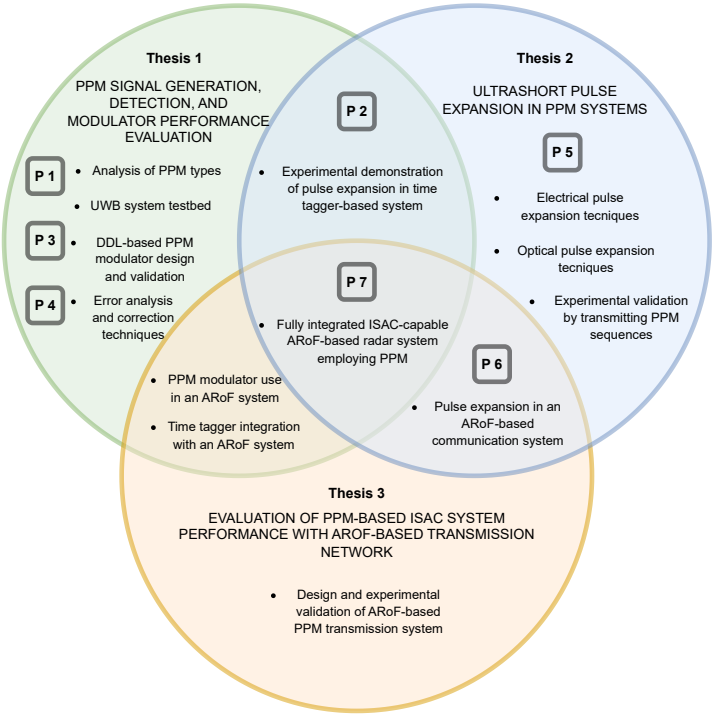


Fig. 1. Diagram of the Thesis structure, where “P” denotes the publications contained within the Thesis.

1 PPM SIGNAL GENERATION, DETECTION, AND MODULATOR PERFORMANCE EVALUATION

1.1 Pulse Position Modulation Types

There are many types of pulse position modulation (PPM) schemes, such as coherent PPM, differential PPM, transmitted reference pulse position modulation (TR-PPM) [73, 74], variable PPM [75], overlap PPM and more [76]. In this Thesis, the following sections focus on coherent PPM, TR-PPM and differential PPM.

Coherent PPM

This Subsection focuses on the coherent PPM following the Consultative Committee for Space Data Systems (CCSDS) recommended standard 142.0-B-1 "Optical communications coding and synchronization" [77]. An example signal structure is shown in Fig. 1.1.

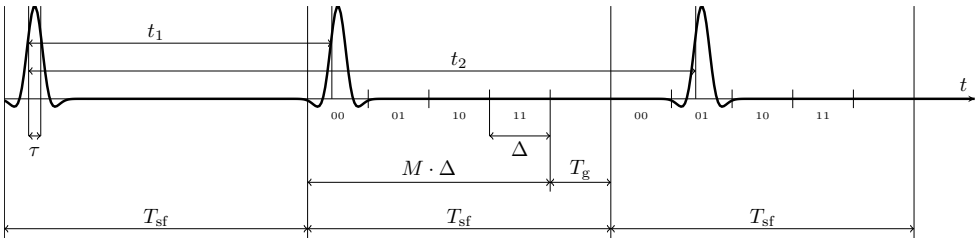


Fig. 1.1. An example coherent PPM signal structure.

In coherent PPM, the sequence of pulses, called a PPM transfer frame, consists of a start pulse, with respect to which all time tags are calculated, and N PPM subframes that contain the data pulses. In a PPM symbol, which is part of the subframe, the pulse can be located in one of M time slots with the slot duration Δ. The number of time slots M is determined by how many bits are encoded in a single PPM symbol, $M = 2^b$, where b is the number of bits per symbol. The total symbol duration is $M \cdot \Delta$. Together with the guard slot duration T_g, the symbol makes up the subframe with the duration [64]

$$T_{sf} = M \cdot \Delta + T_g \,, \tag{1.1}$$

where T_{sf} is the subframe duration, M is modulation order, Δ is the slot duration and, T_g is the guard slot duration.

The guard slot compensates for the hardware's inherent dead time, encompassing signal propagation delays and the duration required for processing, as explored in Section 1.2. The guard slot is added at the end of the subframe as defined in [77] to preserve a clear subframe start at the "0" position. It should be noted that in PPM-based integrated sensing and communications (ISAC) systems, the guard slot is not intended to prevent the reflected echo overlap, as

the received signal's relative time scale is calculated with respect to its start pulse. If multipath propagation is considered, then this aspect becomes relevant, as a delayed replica of the pulse can appear in the next subframe, causing bit errors and erroneous distance calculation.

The time tags for each pulse in the sequence [77] with respect to the PPM transfer frame start pulse can be calculated as

$$t_{\mathrm{k}} = k \cdot T_{\mathrm{sf}} + K \cdot \Delta \,, \tag{1.2}$$

where t_{k} is the time tag with the index k (1 to N) and K is the encoded decimal data (0 to $M-1$) in the subframe.

For this modulation format, the maximum achievable continuous data transfer speed can be calculated by Equation (1.3):

$$R_{\mathrm{b}} = \frac{N \cdot \log_2 M}{(N+1) \cdot T_{\mathrm{sf}} + T_{\mathrm{break}}} \,, \tag{1.3}$$

where R_{b} is the bit rate, M is modulation order, N is the number of symbols in the PPM transfer frame, and T_{break} is the time between subsequent PPM transfer frames.

A custom-built PPM modulator using this technique is presented in Section 1.5, and a full ISAC-capable system is presented in Section 3.2.

Transmitted Reference PPM

This subsection introduces TR-PPM, which uses the same basic principle as described above, and additionally includes a reference pulse at the beginning of each frame that helps to calculate the value of the received symbols. The first time bin starts after $\mathrm{M} \cdot \Delta + T_{\mathrm{g}}$ seconds from the reference pulse. An example of a TR-PPM frame is shown in Fig. 1.2.

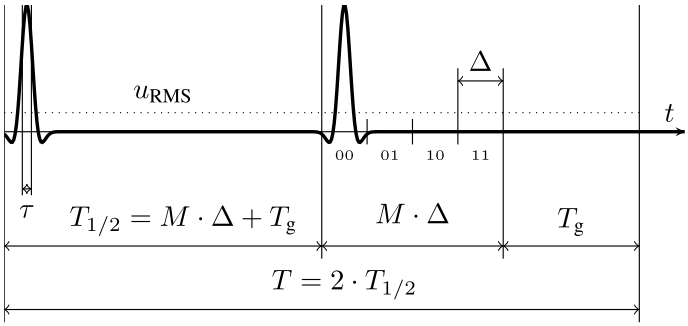


Fig. 1.2. An example TR-PPM signal structure.

The main advantage of TR-PPM is its stability, especially in long-distance transmission, as the time measurement is done between each reference and data pulse pair in the sequence; however, this comes at an efficiency cost, as twice as many pulses are needed to encode the same amount of data.

Differential PPM

This subsection is focused on differential pulse position modulation (DPPM) – one of the most efficient and simple PPM modulation types. It provides higher channel capacity compared to fixed-length symbol modulation types [14]. Using DPPM, a data pulse can be transmitted during every symbol in one of the slots. The difference between the two pulse position techniques is that coherent PPM and TR-PPM send symbols of fixed length, whereas DPPM cuts the part of the symbol that follows the pulse. An example DPPM signal structure is shown in Fig. 1.3.

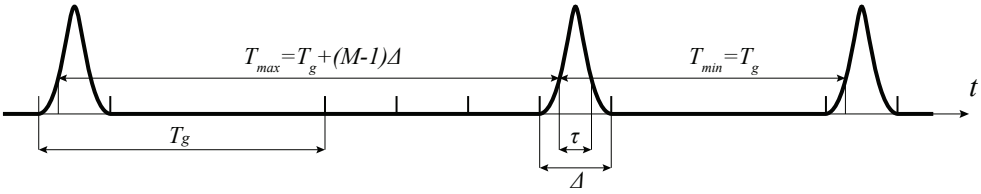


Fig. 1.3. An example DPPM signal structure. ©2023 IEEE

The mean data rate of DPPM can be calculated, considering that M positions are used. The guard interval significantly increases the time between the pulses, especially if the time bin Δ is substantially smaller than T_g. The data rate of the DPPM signal when the guard interval T_g is applied to it can be calculated using Formula (1.4):

$$R_{\text{b,guard}} = \frac{2log_2 M}{2T_g + \Delta(M-1)}. \tag{1.4}$$

The number of data bits within each pulse is determined by the number of time bins utilized in the modulation scheme. For instance, given a pulse coded with N bits, there are $M = 2^N$ possible time bins where the pulse can be positioned within the symbol.

1.2 PPM Signal Detection Methods

Several methods for PPM signal demodulation have been proposed [17, 23, 30, 63, 78, 79]. Correlation receivers are one of the most common approaches to the demodulation of ultra-wideband (UWB) radio frequency (RF) signals [80–84], which is especially attractive in the case of non-coherent TR-PPM [80, 84–86]. More advanced approaches have been developed, including iterative demodulation methods [87] and even chaotic synchronization-based techniques [88]. Advanced methods like compressed sensing (CS) theory can be employed for the demodulation of PPM signals using low-speed analog-to-digital converter (ADC) [89].

One of the most elegant ways to implement a highly efficient PPM demodulator is to employ a time-to-digital converter (TDC) [14, 90, 91]. TDCs are employed in event timers, also known as time taggers, which are widely used in time measurement applications where precise time measurements, and therefore distance measurements, are crucial, particularly for time-of-flight (ToF) measurements [92–97].

In this Thesis, two time taggers (event timers) have been utilized. Eventech A033-ET and Eventech Stream Time Tagger (ESTT) 7 Series. A033-ET can detect events with single-shot root mean square (RMS) resolution better than 5 ps combined with a high measurement rate of up to 20 million events in a burst and featuring a dead time of 50 ns. The incoming events are registered on the rising edge of a low-voltage transistor–transistor logic (LVTTL) signal. This timer can be used for the demodulation of high-order digital PPM signals. The first attempt to use this timer for PPM was made in 2015 [98].

The ESTT features two inputs, thereby enabling ToF and range calculations for ISAC. The event is triggered by a programmatically set voltage threshold value in the range of -2 V to 3 V with a step of 1.2 mV. Different threshold values can be set for the two inputs, allowing the use of signals with varying amplitudes. ESTT features a single-shot RMS accuracy of 1.5 ps and has a dead time of 40 ns, which was the key limiting factor when selecting the PPM parameters, especially the subframe duration T_{sf}. As the ESTT triggers on the rising edge of the pulse, it is critical to have an edge with as short a rise time as possible, but the pulse duration is not crucial, as long as it is above the minimum required duration of 150 ps.

In the presented studies, the PPM demodulation and range data processing were performed in real-time on the personal computer (PC) using custom software. The time tags from the two channels were saved as separate files on the PC, allowing for later processing and range estimation. Additionally, the software enabled saving of the received data for bit error ratio (BER) calculation.

1.3 Digital Discovery-Based Testbed

This section presents the first developed software framework and testbed for exploring PPM communication using short electrical pulses with a duration between 20 ns and 40 ns, employing a high-accuracy event timer for the PPM demodulation.

Experiment hardware consists of a Digital Discovery device, with additional circuitry at digital output pins to provide sufficient signal voltage to ensure that the event timer will receive the incoming signal, an Eventech A033-ET event timer, and a source of white Gaussian noise (WGN). The signal from the Digital Discovery is added to the signal of the WGN generator and sent to the event timer's input.

A Python script performs communication with the Digital Discovery device using WaveForms software development kit (SDK) and the A033-ET event timer using TCP/IP messages. The software diagram is presented in Fig. 1.4.

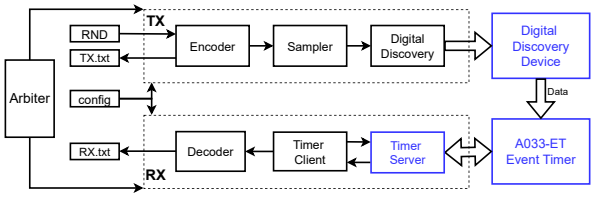


Fig. 1.4. Testbed software layer diagram. ©2022 IEEE

Verification of the testbed has been performed using transmission of pseudorandom binary sequence (PRBS), encoded using the TR-PPM scheme with $\Delta = \tau$ and $M = 32$. Pulse duration and duration of the time slot are limited by the sample rate of the Digital Discovery. The number of symbols in the packet was selected based on the event timer's limitations. It can detect 64 pulses at a time, so no more than 31 symbols can be sent, considering the empty symbol with one pulse and payload symbols with two pulses. The Guard time was 40 ns. The additive WGN has been controlled manually with 10 mV RMS step. The experimental results are presented in Fig. 1.5.

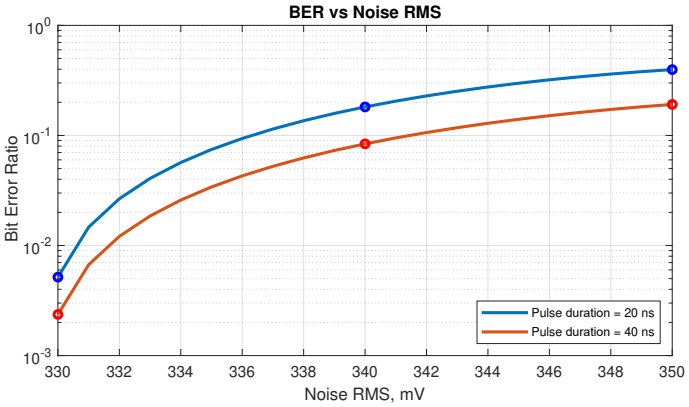


Fig. 1.5. BER as a function of noise RMS for pulse durations 20 ns and 40 ns. ©2022 IEEE

The first errors appear at 330 mV RMS and continue to rise as the noise intensity increases. The use of 40 ns pulses leads to a lower bit-error rate than the 20 ns pulse sequence. With 20 ns pulses the signal RMS is approximately 730 mV, whereas with 40 ns it is 980 mV. Moreover, the signal waveform is imperfect and oscillates.

The jitter of the pulses increases as the signal-to-noise ratio (SNR) of the signal decreases. At SNR = 13 dB it is 1.1 ns, and at SNR = 7 dB it is 2.6 ns. The main reason why the BER starts to rise is that the timer has a threshold voltage of around 1.2 V at which it reacts to incoming pulses. The jitter of the rising edge does not exceed 2.8 ns. Therefore, the jitter does not affect the timer's decisions and does not decrease BER in the presented setup.

The presented testbed served as an important stepping stone in PPM research, and **the full publication can be seen in [66] ©2022 IEEE.**

1.4 Ultrashort Slot Duration Differential PPM

This section presents DPPM modulation scheme and demonstrates possibilities for demodulation of DPPM using the highly accurate A033-ET event timer, demonstrating data transmission using a high-order DPPM signal in a laboratory environment.

The DPPM signal generation is achieved using the Keysight M8195A arbitrary waveform generator (AWG), featuring a 25 GHz analog bandwidth and a 65 GSa/s sampling rate, which is a significant upgrade from the Digital Discovery device presented in the previous section. The AWG allows for the PPM duration to be as short as 100 ps, significantly increasing the energy efficiency in the transmission channel. The A033-ET event timer served as the PPM demodulator. Since the event timer cannot detect such short pulses, a custom pulse expansion module (PEXM) was employed that contains the following hardware in the following order:

1) 6 dB RF attenuator to remove possible back-reflection from custom low-pass filter (LPF);
2) In-house manufactured custom LPF [99];
3) VLFX-1300+ commercial LPF,
4) 30 dB RF amplifier with bandwidth 30-4000 MHz;
5) SHF BT45 broadband bias tee with bandwidth 20 kHz - 45 GHz.

The full experimental setup, including the PEXM, is shown in Fig. 1.6.

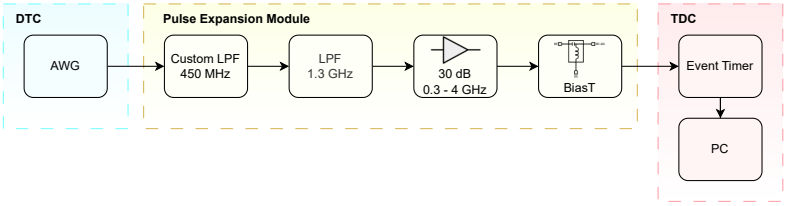


Fig. 1.6. Experimental setup for DPPM transmission including PEXM. ©2023 IEEE

The software framework, presented in Section 1.3, was employed. The event timer received the signal sequence with DPPM pulses at specific absolute times (also known as time tags). From each time tag, guard time T_g was subtracted, and the resulting time was divided by slot duration Δ, obtaining relative time tags converted to the pulse positions. Finally, the positions were reversed to binary data.

Experimental validation was performed by transmitting PRBS with parameters shown in Table 1.1. Each experiment consisted of one transmitted data packet of 63 data pulses. To ensure that a valid output signal was obtained, a periodic sequence of 100 ps pulses was transmitted before data transmission. Each experiment file was loaded in AWG individually. At the same time, the event timer was being configured for event measurement. The AWG generated pulse was expanded by the PEXM to about 750 ps, which is an optimal and valid signal width for event detection.

Table 1.1 summarizes the results of decoded DPPM test signals where BER was calculated for each test. The test did not detect any bit errors at slot duration $\Delta = 200$ ps. At 100 ps and 50 ps the error rate increases significantly $1.781 \cdot 10^{-2}$ and $7.935 \cdot 10^{-4}$, accordingly.

Table 1.1

DPPM Transmission Experimental Parameters and Results ©2023 IEEE

Test nr.	**τ, ps**	**Δ, ps**	**M**	**T_g, ns**	**Total bits**	**BER**
1	100	200	128	50	4410	0
2	100	100	256	50	5041	$7.935 \cdot 10^{-4}$
3	100	50	512	50	5670	$1.781 \cdot 10^{-2}$

The implemented DPPM transmission test setup has demonstrated excellent results, as indicated by the low bit error rate observed. Despite the jitter and systematic timing error, the test system could accurately detect the pulses with an error rate of no more than one position.

Full description can be seen in [67] ©2023 IEEE.

1.5 Digital Delay Line-Based PPM Modulator

Development of a more capable means of PPM generation was the logical next step in the presented research. This section presents the design and validation of custom-built PPM modulators based on digital delay line (DDL) technology, which offer advantages over widely used field-programmable gate arrays (FPGAs) for PPM signal generation [100], and other hardware-based pulse generators [3], which are limited in available PPM slot width and accuracy.

DPPM Modulator

This subsection is focused on the design, implementation, and testing of a modulator intended for DPPM applications. The novelty of the proposed modulator lies in the implementation of a DDL-based digital-to-time converter (DTC) for the modulation of the PPM signal. The employment of this technology allows the integration of software-defined radio (SDR) concepts [101, 102] to UWB, which, in turn, allows to easily switch between different PPM modulation formats and bandwidths.

A custom printed circuit board (PCB) has been developed for generating PPM signals, which is controlled by a PC. The main components of the modulator are the MC100EP196B high-precision programmable DDL, SI5394J-A phase locked loop (PLL) jitter attenuator and Cyclone IV FPGA system-on-chip (SoC).

The Altera Cyclone IV FPGA SoC controls and commands the modulator. FPGA was chosen because of its high-speed digital logic capabilities. It interprets the commands and serves as an interface between the PC and the rest of the modulator board. The software architecture of the

FPGA SoC part of the modulator is implemented as a Nios II virtual processor with custom IO procedures written in VHDL.

The MC100EP196B high-precision programmable DDL has a maximum time resolution of 10 ps and a programmable range of 10450 ps when using all data inputs (D0 to D9). The total delay range of the DTC is 2.2 ns to 12.4 ns, including the minimum fixed delay.

For each PPM symbol, a pulse is generated based on the 10 MHz reference clock, which can be delayed in 10 ns increments (coarse delay) and also delayed by the DDLs to achieve fine control over the pulse location in time (precision delay).

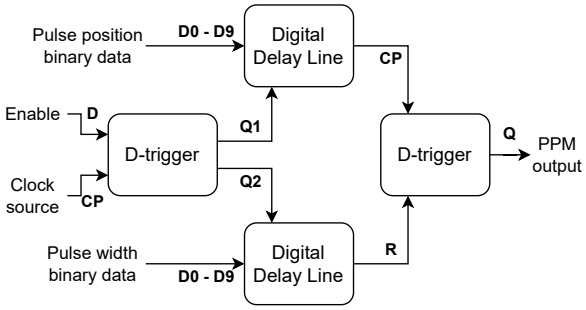


Fig. 1.7. Block diagram of the DDL-based modulator implementation. ©2024 IEEE

The testing of the modulator was carried out by directly connecting its output to the ESTT 7 Series event timer. The block diagram of the connection scenario and full software stacks is shown in Fig. 1.8.

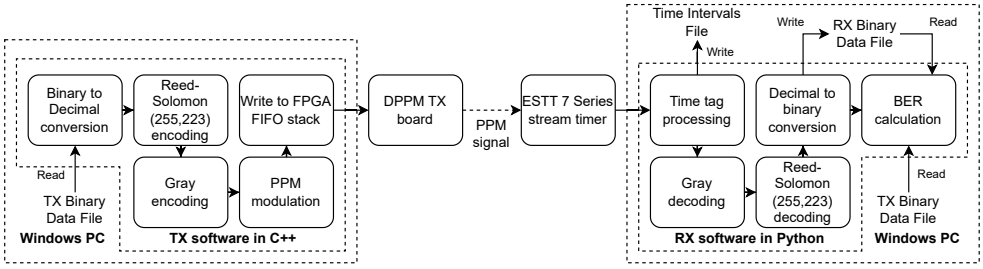


Fig. 1.8. DPPM transmission test setup block diagram. ©2024 IEEE

The jitter distribution shown in Fig. 1.9 was obtained by analyzing the deviations of measured pulse positions from expected ones. The resulting RMS of pulse position deviation was 18.9 ps. Considering that the jitter distribution is close to normal, 99.7 % of deviations fall within the 3σ range, i.e., 56.7 ps.

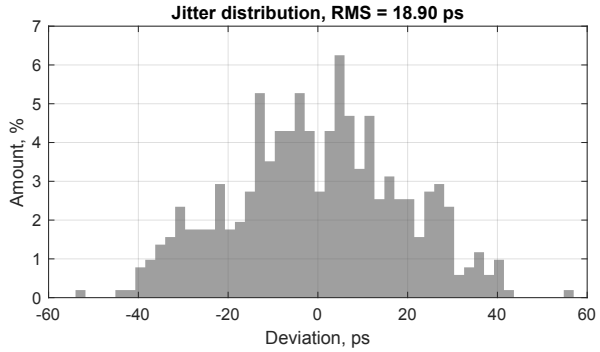


Fig. 1.9. Modulator jitter distribution measured by the ESTT. ©2024 IEEE

For the data transmission tests, a PRBS was used with a length of one million bits and encoded using DPPM, with $t_g = 50$ ns and $\tau = 150$ ps. The impact of different time bin duration values and number of positions with various forward error correction (FEC) codes has been explored, and BER calculated for each case. The experimental results in Fig. 1.10.

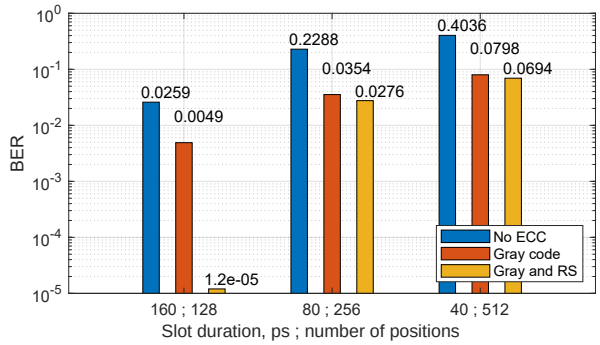


Fig. 1.10. Experimental results for DPPM transmission tests. ©2024 IEEE

The results show that the designed modulator provides real-time data communication, and the implemented error correction algorithms are working as intended. The most significant impact on the BER is achieved using the Gray code, further enhanced by the Reed–Solomon (RS) error correction algorithm. When combined, these error correction schemes provide a BER of $1.2 \cdot 10^{-5}$ at a slot duration of 160 ps. Even for an extremely small 40 ps slot duration, using error correcting code (ECC), it is possible to reduce BER to 0.07, which can be further reduced using more advanced codes, such as low-density parity check (LDPC).

Considering the guard time, the presented modulator using the DPPM scheme can theoretically achieve a data rate up to 149 Mbit/s using 512 positions and a slot duration of 40 ps. In practice, the developed transceiver prototype achieved a real-time transmission speed of about 10 Mbit/s due to PC software limitations.

Full description can be seen in [68] ©2024 IEEE.

Coherent PPM Modulator

This subsection presents the design of the next evolution of the DTC-based PPM modulator, which utilizes the same core component – DDL. The conceptual diagram of the DTC is shown in Fig. 1.11. The device is compliant with CCSDS recommended standard 141.0-B-1 "Optical communications physical layer" [103].

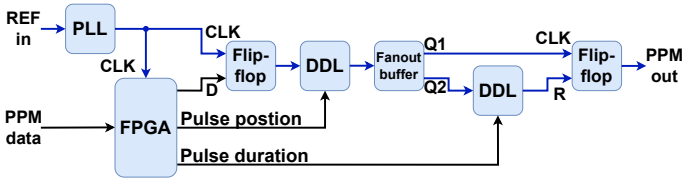


Fig. 1.11. Conceptual block diagram of the PPM modulator.

The core of the DTC is the MC100EP196B programmable DDL with the programmable delay range 0–10.24 ns in 10 ps increments, and it features a ±11 ps linearity across the whole delay range. The purpose of the DDL is to delay a pulse at its input by a specified time interval, set via the 10-bit-wide input bus, allowing 1024 unique delay values.

The DTC is controlled by the Altera Cyclone IV FPGA, which is connected to the PC via a USB 3.0 interface. Each PPM symbol in the transfer frame is stored at a separate memory address as a 24-bit binary number, where 10 bits specify the pulse delay from the start of the current clock cycle and 14 bits specify the number of clock cycles until the next pulse in the sequence. At the start of the PPM transfer frame, a start pulse is generated, from which the clock cycles are counted. At this time, the FPGA also already prepares and outputs the 10-bit delay value for the next pulse in the sequence. When the FPGA receives a set number of clock cycles (14 bits in the memory address), it generates a single pulse which is delayed by the value already set in the DDL. Then the FPGA moves to the next memory address, where the data for the next pulse in the sequence is stored, and the same process repeats until the end of the PPM transfer frame.

The device can transmit a 16000-symbol-long PPM transfer frame at a time, with about 20 ms between PPM transfer frames, a software limitation that can be further improved to significantly increase the continuous data transfer rate. For example, with $M = 16$ and $\Delta = 100$ ps, the modulator can achieve a data transfer speed of 2 Gbit/s if the guard slot duration and break are nearly eliminated.

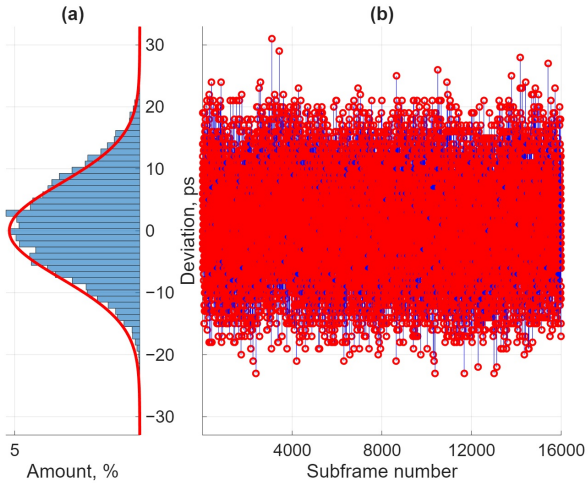


Fig. 1.12. Jitter distribution test results for the developed modulator: (a) jitter distribution; (b) pulse deviation from ideal positions.

The testing of the modulator was performed by connecting the modulator directly to the ESTT via a coaxial cable, in an electrical back-to-back (B2B) configuration. The jitter distribution and pulse position deviation from expected values over a 16000-symbol-long PPM transfer frame are presented in Fig. 1.12. The red line in Fig. 1.12 (a) represents the distribution of jitter. As can be observed, the pulse position jitter is approximately normally distributed, with a RMS jitter of 7.65 ps.

The presented modulator is employed in research shown in [72].

1.6 Error Analysis and Correction Techniques

FEC is widely used in PPM-based communication systems that use transmission channels that are noisy and can be unreliable. Furthermore, the errors in the received information tend to increase when moving closer to the limits of the data transmission capacity for the channel. The FEC algorithm must be selected depending on the application and computational capabilities of the communication modem.

This section is devoted to the theoretical study and simulation of custom error-correction algorithms in conjunction with FEC for the improvement of TR-PPM transmission links [104]. In this section, major PPM link degradation reasons and respective mitigation methods are investigated. Special attention is paid to FEC methods and their suitability for PPM communication links. A theoretical framework describing the impact of jitter and systematic errors, such as clock drift, on the performance of PPM link is developed. Using computer simulation, the contribution of Gray coding and RS coding to the reduction of BER of TR-PPM communication link with an event timer-based demodulator is found.

Theoretical Framework

In setups where PPM slot duration below 100 ps is used, it is challenging to maintain precision due to various conditions that can cause position errors. For instance, temperature can affect the internal circuitry, which generates clock signals, resulting in position errors. Additionally, errors may occur as a result of the inability of the generator to provide an exact clock divisor, leading to tiny pulse shifts in time.

Moreover, these errors can arise if a jitter is introduced in the signal, causing the receiver to detect the pulse position differently from what was expected. Earlier tests [105] and Section 1.5 of this Thesis have shown that the values of the jitter are distributed approximately normally. The BER of PPM data transmission can be found via calculation of the probability of the pulse appearing at different positions using Formula (1.5).

$$P(\sigma, \mu) = 1 - \int_{-\frac{1}{2}\Delta}^{\frac{1}{2}\Delta} \frac{1}{\sigma\sqrt{2\pi}} e^{-\frac{1}{2}(\frac{x-\mu}{\sigma})^2} dx, \tag{1.5}$$

where x is the deviation from ideal position, μ is systematic error caused by the clock drift, and σ is standard deviation of the jitter. For the normal distribution function, 99.73 % of cases are within $\pm 3\sigma$ interval. If the jitter is limited in range $(-t_j/2, t_j/2)$, using the 3σ rule, the standard deviation can be found as $\sigma = t_j/6$, where t_j is the jitter amplitude.

If the PPM signal structure where bits per symbol $N = 8$ is used, and a position error occurs where the time drift does not exceed $\frac{3}{2}\Delta$, then a one-bit error will be determined in 8-bit symbol. If deviation x does not exceed one position, and it leads to only a 1-bit error, the BER B can be calculated by using Formula (1.6):

$$B(\sigma, \mu) = \frac{P(\sigma, \mu)}{N} = \frac{1}{N} - \frac{1}{N} \int_{-\frac{1}{2}\Delta}^{\frac{1}{2}\Delta} \frac{1}{\sigma\sqrt{2\pi}} e^{-\frac{1}{2}(\frac{x-\mu}{\sigma})^2} dx. \tag{1.6}$$

Due to the high probability of position error if $t_j \geq \Delta$, appropriate FEC codes should be implemented. If the PPM pulse is detected in a different position, the binary code of the symbol will change with respect to the new position. Employment of Gray coding of the PPM positions ensures that one position shift will result in a single-bit error.

Validation of Error Correction Algorithms

A simulation was performed in the MATLAB environment and employed experimentally determined jitter and clock drift values of the custom-designed modulators presented in Section 1.5. In the hardware prototypes, the deviation of the data pulses from their expected positions was distributed semi-normally. In contrast, the errors introduced by the clock drift were almost constant during one PPM frame. As the clock drift does not significantly increase for the duration of the PPM sequence, it can be modeled as a constant offset from the expected data pulse position values.

In the simulation, the RS error correction algorithm was implemented. The RS(255, 223) code was used, in which a block consists of 223 data bits with 255 total bits. The simulated RMS jitter ranges were 10–22 ps and 30–55 ps. The position count in all experiments was 256 and the slot duration 155 ps. The transmitted data was generated as a 255-symbol-long (8 bits per symbol, 1784 total bits) PRBS and encoded using RS(225, 223) code and Gray code, if applicable for the specific experiment.

The event timer was simulated by adding 3 ps RMS jitter to the simulated received data. The experimentally obtained BER as a function of RMS jitter for the previously mentioned error correction schemes without clock drift error can be seen in Fig. 1.13 and with added clock drift error in Fig. 1.14.

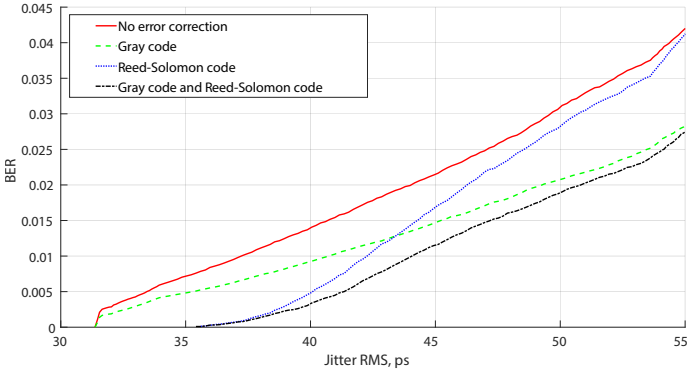


Fig. 1.13. Simulation results without clock drift error. ©2024 IEEE

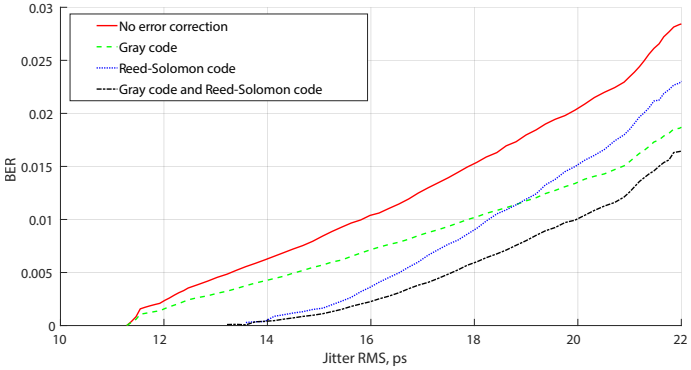


Fig. 1.14. Simulation results with added clock drift error. ©2024 IEEE

The results show that the RS error correction scheme performs well up to a jitter RMS of about 45 ps. The Gray code provides the most significant decrease of the BER as it provides for a single bit error in the PPM symbol in case the data pulse is shifted by a value equal to or less than one slot duration.

FEC based on RS code allows for the reduction of bit errors caused by both jitter and clock drift. However, after a certain point, RS code cannot correct the bit errors caused by the jitter

since RS(255,223) code can correct 16 bit errors per block. For this reason, data should also be encoded using Gray code, since it improved in BER over the whole range of jitter RMS.

Full description can be seen in [69] ©2024 IEEE.

1.7 Summary of the First Thesis

The first thesis was devoted to proving that a PPM modulator implemented using programmable gate and multiplexer-based DDL integrated circuit (IC) technology is capable of achieving PPM pulse sequence generation with RMS timing jitter below 10 ps. To achieve this objective, a testbed was developed to research concepts used in PPM data transmission; high-precision time-taggers were tested and validated for use in PPM systems, and for the first time, a data transmission experiment using PPM and a time-tagger intended for satellite laser ranging (SLR) applications was performed. Two MC100EP196B high-precision programmable DDL-based modulators were developed and tested using the ESTT, at first achieving an RMS jitter of 18.9 ps and the latter model 7.65 ps, thereby proving the thesis. The developed modulator can transmit a 16000-symbol-long PPM transfer frame at a time, with about 20 ms between transfer frames, using slot durations as low as 10 ps and modulation order above 256. Data transmission experiments showed a BER as low as 1.2×10^{-5} using Gray and RS code. The testing revealed that the jitter is distributed approximately normally, and finally, the systematic errors were analyzed and correction techniques proposed.

Full description of the results presented in this chapter can be seen in [66], [67], [68], [69], and [72].

2 ULTRASHORT PULSE EXPANSION IN PPM SYSTEMS

The demodulation of a PPM signal employing extremely short pulses is challenging as it requires fast electronic circuitry, such as comparators and triggers with bandwidths of tens of gigahertz. As PPM pulse duration does not carry information, the problem can be tackled by increasing the duration of the received pulses just before the demodulation. The occupation of several time positions by the single incoming expanded pulse does not create any issues with PPM demodulation, as only the rising edge of the pulse carries the information. Also, there is no stringent requirement to maximally preserve the shape of the generated pulse being transmitted via a channel to the receiver unit, provided that the pulse shape variations do not vary considerably between the pulses; one only needs to ensure that the change in the pulse shape is not too significant to provide correct demodulation.

This chapter focuses on the expansion techniques of 50–100 ps short pulses using passive electrical and optical devices for subsequent use in PPM demodulators and demonstrates that passive techniques can be successfully applied for high-bandwidth pulse expansion in both optical and electrical domains. Employment of electrical LPF and optical techniques, namely, fiber Bragg grating (FBG), for pulse duration expansion is explored.

2.1 Electrical Pulse Expansion

Many modern electrical and optical systems, such as UWB communication devices, signal processing circuits, radar systems, and more, are dealing with the transmission, measurement, and processing of short pulses [106, 107]. These operations often require the pulse to be expanded or compressed with minimal waveform distortion. Various delay lines [108–112] and other devices operating in the frequency domain (for example, filters) and making changes to it [113–123] and combinations of delay lines and filters are widely used for pulse expansion. Both digital and analog signal processing techniques are used, and each has advantages and disadvantages.

An option for pulse shaping involves using filters that influence the pulse magnitude spectrum. Passive and active filters [124, 125] can be utilized for this purpose. The simplest active filters are built around transistor and op-amp circuits as their fundamental components [126], although, in most cases, they tend to be more complex [127]. Active filters offer greater flexibility, allowing for reconfigurable bandwidths ranging from narrow/mid-band to ultra-wideband states, as described in [128].

To ensure an unambiguous event timer response and the minimum possible jitter in time interval detection as well as the stable operation of the event timer and initial state recovery, it is necessary to ensure that the initial pulse is extended to about 150 ps, that the filtered pulse does not have noticeable ripples or a long tail, and that the rising edge of the filtered pulse is preferably as steep as possible.

Analytical derivations and numerical modeling in [99] have confirmed that, of all the filter types, the Bessel-type filter is the most suitable for pulse expansion, as it has a maximally flat

group delay and a maximally linear phase response. Those characteristics ensure negligible ringing in the impulse response [129] and minimize overshoots in the pre-transition and post-transition aberration regions of the expanded PPM pulses.

Experiments were performed with commercially available LPFs to determine if an off-the-shelf filter could be used for pulse expansion. An example of pulse expansion using the Mini-Circuits SLP-2400+ filter [130] is shown in Fig. 2.1. The commercial filter introduced noticeable oscillations in the post-transition region. Moreover, it significantly flattened the pulse's rising edge, increasing the timer's sensitivity to the additive noise.

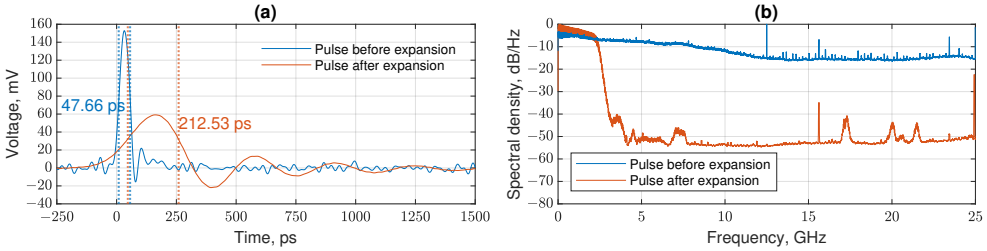


Fig. 2.1. Pulse expanded using Mini-Circuits SLP-2400 filter: (a) waveforms of the pulses; (b) normalized magnitude spectra.

Custom-Built Electrical Pulse Expanders

Two microstrip LPF filters were designed to extend the pulse duration from 50 ps up to about 170 ps, which is slightly above the event timer's minimum pulse duration threshold of 150 ps, to ensure that the timer will definitely respond. Analytical and numerical calculations, computer modeling, and measurements showed that the third-order Bessel LPF capacitor–inductor–capacitor filter, which is normalized by the group delay (hereafter called Classical), is the most suitable for the expansion task. The normalization of the second filter (hereafter called Magnitude-Normalized) was performed using the traditional magnitude normalization methodology, where the gain is -3 dB at the cutoff frequency. The filters are shown in Fig. 2.2.

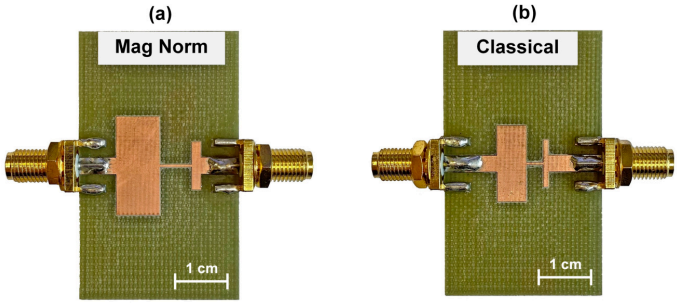


Fig. 2.2. Custom-designed filters: (a) Magnitude-Normalized, and (b) Classical, with cutoff frequencies $f_c = 1.8$ GHz.

Simulated and measured curves of the group delay for both filters are shown in Fig. 2.3. The

group delay curves obtained in the simulation and the experimental ones are in good agreement if the slopes of the curves are compared.

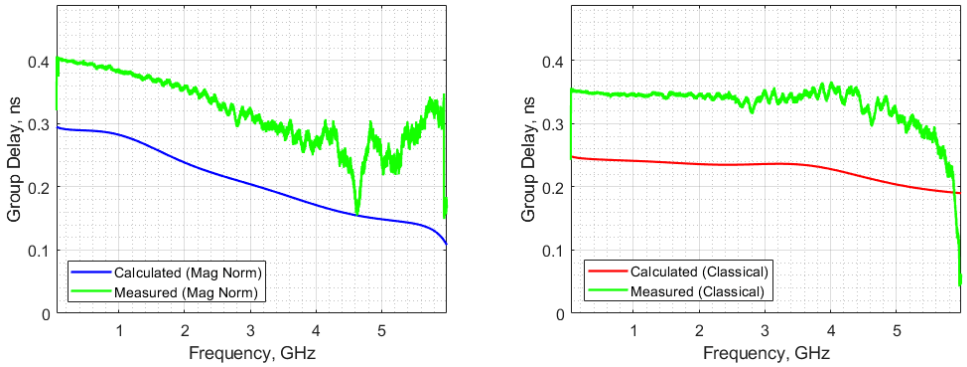


Fig. 2.3. Ansys HFSS simulation results and custom-designed filter measurement results for group delay.

The results of a 50 ps input pulse expansion by the Classical LPF filter can be seen in Fig. 2.4, whereas those of the Magnitude-Normalized LPF filter can be seen in Fig. 2.5.

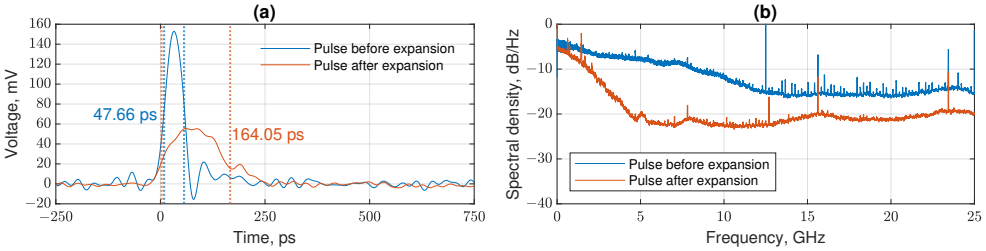


Fig. 2.4. Pulse expanded using Classical custom-designed filter: (a) waveforms of the pulses; (b) normalized magnitude spectra.

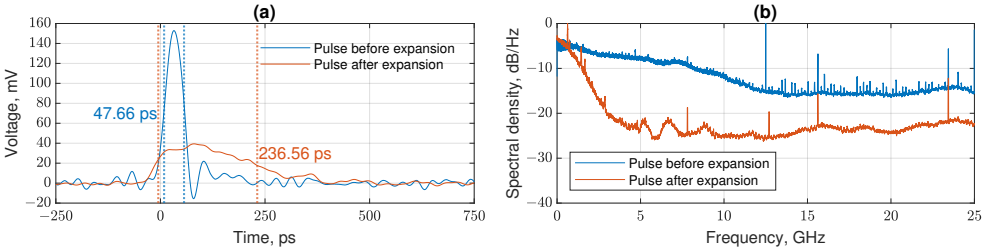


Fig. 2.5. Pulse expanded using Magnitude-Normalized custom-designed filter: (a) waveforms of the pulses; (b) normalized magnitude spectra.

It can be seen that the pulse expanded by the Classical filter to 146 ps is close to the desired pulse waveform, as it meets the waveform requirements. The Magnitude-Normalized filter expands the pulse to 237 ps, and this pulse waveform has a first transition duration that is too large, a long tail, and ripples in the tail.

2.2 Optical Pulse Expansion

PPM pulses can be expanded not only in the electrical domain but also in the optical domain when signal transmission over optical fiber is realized. To increase optical pulse duration, so-called optical pulse stretchers or techniques are used [131–134]. In general, pulse stretchers can be classified into two categories: coherent and incoherent. Coherent pulse stretchers, such as grating pulse stretchers, stretch a pulse in a way that can later be undone. They provide positive or negative group delay dispersion and typically are based on dispersive elements like diffraction grating pairs, grisms (grating and prism), FBG, chirped Bragg gratings, or ring resonators. On the other hand, incoherent pulse stretchers irreversibly stretch a pulse [131, 132, 135]. In the presented experiments, a tunable FBG to introduce positive dispersion and broaden the input optical PPM pulses was used, as shown in Fig. 2.6.

The target of this experiment was to expand 50 ps optical PPM pulses up to at least 150 ps. This is necessary as the duration of the incoming PPM pulse on the input of the event timer should be at least 150 ps to provide stable operation.

The tunable FBG was set to the chromatic dispersion (CD) value of +1200 ps/nm, which was equal to around the dispersion value introduced by 75 km of standard ITU T G.652 single-mode optical fiber (SMF). As a result, FBG set to this value of CD expanded the PPM pulses up to 154.03 ps, as shown in Fig. 2.7. It can be concluded that FBG behaved as a slight band-rejection filter with a center frequency around 6 GHz.

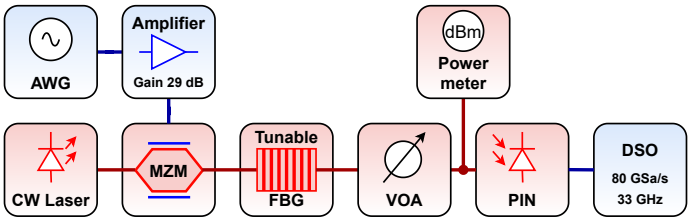


Fig. 2.6. Block diagram of optical pulse expansion test setup.

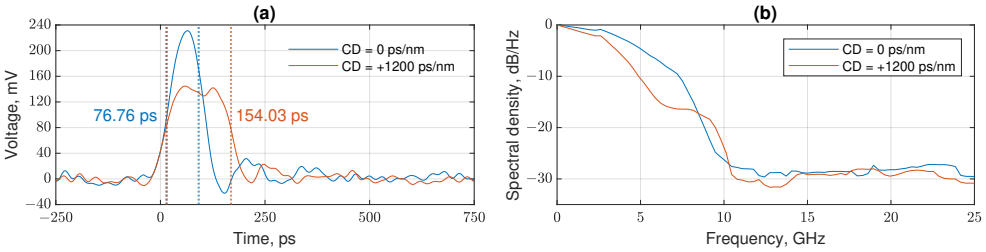


Fig. 2.7. Pulse expanded using tunable FBG: (a) captured waveform, and (b) normalized magnitude spectra.

The experiment successfully demonstrated the optical pulse expansion capacity of the tunable FBG module.

2.3 Pulse Expansion Method Experimental Validation

The PPM transmission experiments have been carried out using optical and electrical pulse expansion methods with TR-PPM waveforms. The PPM pulses were kept as short as possible to demonstrate energy-efficient transmission.

The block diagram of the PPM transmission system is illustrated in Fig. 2.8. Key components of the system are a pulse expander module (optical FBG or electrical LPF) and a high-precision event timer used for the demodulation. AWG acts as a PPM transmitter, generating the desired signal waveform following our loaded sampled data. Unipolar PPM pulses with a time duration of 50 ps were used. When pulse expansion was realized by the LPF, the CD value of FBG was set to 0 ps/nm.

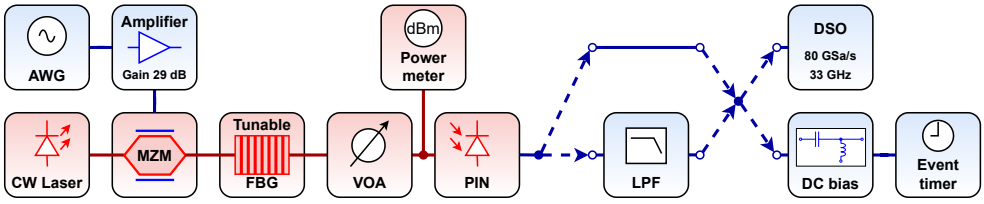


Fig. 2.8. Block diagram of a PPM transmission link with an event timer for the demodulation.

The experiment has been conducted using TR-PPM waveforms [74] with the parameters listed in Table 2.1 by employing optical or electrical pulse expansion methods. In both cases, BER measurements were relative to the average optical power received before the photodetector (PD). The BER versus the average received optical power with optical pulse expansion for multiple slot duration values is shown in Fig. 2.9, whereas in the case of electrical pulse expansion, the results can be seen in Fig. 2.10. The range of the average received optical power values was selected to represent the region around which the data transmission transitions from error-free to completely unintelligible (BER value of 0.5). This range was experimentally determined for the given system and corresponds to the amplitude values of the electrical pulse on the edge of the detection threshold of the event timer.

Table 2.1

TR-PPM Transmission Experiment Parameters

Number of positions, N	**Slot duration Δ, ps**	**Pulse duration τ, ps**	**Expansion method**
512	50	50	Optical
256	100	50	Optical
128	200	50	Optical
512	50	50	Electrical
256	100	50	Electrical
128	200	50	Electrical

The FEC limit represents the BER threshold at which the Reed–Solomon RS(255, 223) FEC

algorithm is capable of correcting the errors in the received data pattern. This BER value is 6.27×10^{-2} as the RS(255, 223) algorithm can correct up to 16 erroneous symbols in the block.

For the experiments conducted using a slot duration of 200 ps, the results reveal a distinct point where the data transmission becomes error-free. This happens when the incoming PPM signal at the input of the event timer significantly exceeds the threshold set by the direct current (DC) bias voltage so that no adverse effects, such as noise and jitter, significantly impact the BER. In contrast, if the magnitude of the incoming pulses, which corresponds to a certain average received optical power, falls below the voltage threshold of the event timer, very low BER values are observed in all cases. The threshold effect is observable at a slot duration of 200 ps. In contrast, in the case of slot durations of 50 and 100 ps, the experiments show an error floor, especially in the case of optical pulse expansion. This is expected behavior, as smaller slot durations require more precise modulation in the transmitter and demodulation in the receiver. Adverse effects such as jitter and additive noise in all system components considerably impact the PPM signal with smaller slot durations. As the slot durations of PPM pulses decrease, the jitter can more likely cause the estimated pulse position in the receiver to shift to a different pulse position than the one generated by the modulator.

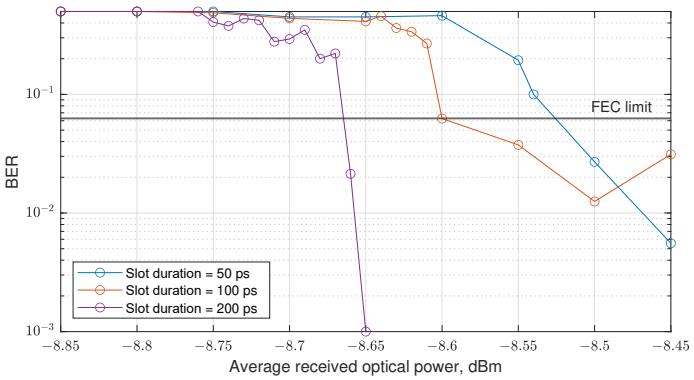


Fig. 2.9. BER versus average received optical power with optical pulse expansion with FBG module.

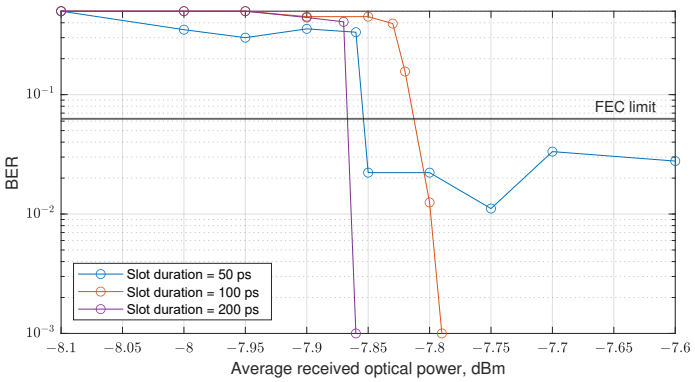


Fig. 2.10. BER versus average received optical power with electrical pulse expansion with LPF.

The results validate the concept of both electrical and optical pulse expansion methods for use with the event timer, as the BER values, even at very small slot durations of 50–100 ps, are acceptable. The lower BER values in the case of electrical pulse expansion at a similar average received optical power can be attributed to the excellent pulse shape at the output of the custom LPF, which leads to higher accuracy in the triggering of the event timer, resulting in less error-prone transmission. Employment of new pulse expansion techniques in conjunction with a more capable TDC allowed to achieve a much lower BER compared to the results presented in [104].

2.4 Summary of the Second Thesis

The second thesis was devoted to proving that in time tagger-based PPM systems, a pulse with duration 50–100 ps can be expanded passively by electrical and optical means to more than 2 times its original full width at half maximum (FWHM) duration while preserving the pulse's waveform shape enough for stable detection. In this chapter, two methods of passive pulse expansion were discussed: electrical and optical. A commercial Mini-Circuits SLP-2400 LPF was tested and found to have expanded the 47.66 ps pulse to 212.53 ps with noticeable ripples in the falling edge. Two custom-built filters were presented and tested, achieving expansion to 164.05 ps and 236.56 ps, respectively; however, in the latter case, the falling edge was highly stretched. Optical pulse expansion using an FBG was experimentally tested, stretching the pulse to 154.03 ps with excellent waveform shape. Both methods were validated in experiments involving data transmission in an optical PPM communication system, achieving BER values below 1×10^{-3}.

Full description containing the results presented in this chapter can be seen in [70].

3 EVALUATION OF PPM-BASED ISAC SYSTEM PERFORMANCE WITH AROF-BASED TRANSMISSION NETWORK

Achieving tight sub-nanosecond timing tolerances required for distributed sensing, especially in PPM applications, is challenging. To address this issue, fiber-optic technologies provide low-jitter, long-distance physical links with an established functional model: radio-over-fiber (RoF) [136, 137]. RoF has gained considerable popularity, as optical fiber links and passive optical network (PON) infrastructure are deployed to consolidate these technologies in centralized radio access network topologies [138–140]. Additionally, RoF has already proven itself to be a valuable addition to interconnected radar architectures [141], enabling simplified radar data transmission [142–144]. A sub-branch of RoF, analog radio-over-fiber (ARoF), further simplifies the system by sending an analog signal directly over an optical fiber without analog-to-digital conversion. This approach preserves the signal's continuous form and analog nature, which can be beneficial for subsequent signal processing and synchronization, especially in PPM-based systems, which require high timing accuracy. Consequently, ARoF technology has been explored in recent research for millimeter-wave [145, 146] and terahertz links [147, 148]. Additionally, ARoF is being considered for future distributed multiple-input multiple-output (D-MIMO) systems in 6G networks [140, 149–153], as well as wireless communications, distributed sensor networks, radars, space communication systems, and many other applications [154–157].

This chapter is focused on the design, implementation, and evaluation of PPM-based communication systems using the ARoF technology for long-distance optical signal transmission, and exploring range measurement capabilities in an ISAC system that uses a time tagger as the demodulator.

3.1 Design and Evaluation of 28 GHz Microwave/Optical Transmission System Utilizing PPM

This section presents a novel, experimentally validated communication system employing TR-PPM transmission over ARoF. In this implementation, the central office is equipped with a local analog RoF transmitter; in turn, the base station consists of a remote antenna unit (RAU) serving as the RF transmitter in the access network. The demodulation of PPM signal is performed by TDC based on a commercial event timer. The presented system functions as a testbed for the investigation of impulse radio ultra-wideband (IR-UWB) communication and future use cases of UWB ISAC.

Experimental Setup

The experimental system mainly consists of three parts: (a) ARoF transmitter, (b) RAU transmitter, and (c) RAU receiver, as shown in Fig. 3.1.

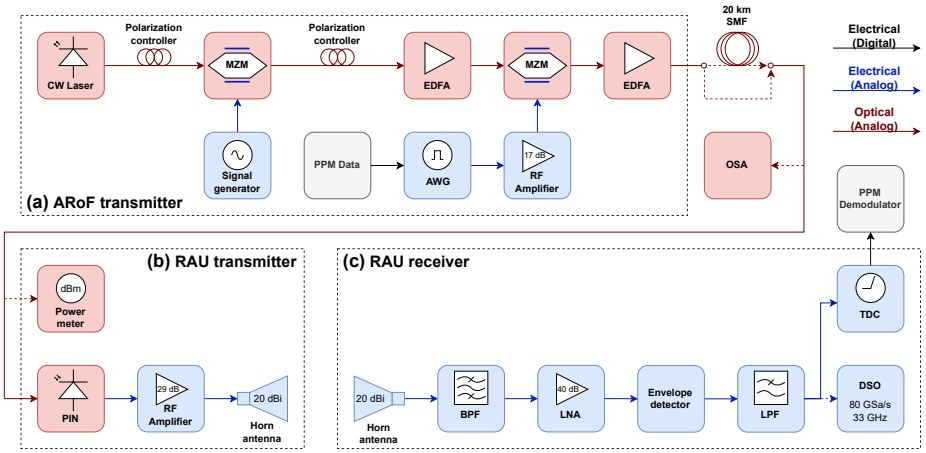


Fig. 3.1. Experimental setup of the PPM-based ARoF communication system.

In the setup, the optical output (1550 nm wavelength) from a continuous wave (CW) laser was first directly connected to a Mach–Zehnder modulator (MZM). The bias point was adjusted near its zero level. A sinusoidal signal generator, producing a 14 GHz sinusoidal electrical signal, was directly connected to the electrical signal input of the first MZM. As a result, the desired RF of 28 GHz was achieved between the generated tones in the optical domain at the output of the first MZM. The output of the first MZM, comprising two equal optical tones (carriers) spaced 28 GHz apart, was subsequently amplified using an erbium-doped fiber amplifier (EDFA) and then modulated with the TR-PPM waveform using a second MZM. The TR-PPM waveform was generated using the Keysight M8195A AWG.

An optical signal pre-amplification by a second EDFA with an optimized gain was performed before launching the optical signal into a 20 km long ITU-T G.652 rec. compliant SMF span. As for the optical receiver, a PD was used, which realized the photodetection-based RF generation from the optical beat note. The RF signal output power from the PD was amplified before being transmitted to the Ka-band horn-type antenna.

The receiver was located 5 m away from the RAU transmitter. The transmitted mm-wave signal was received by an identical Ka-band antenna and filtered using the bandpass filter (BPF). After filtering, the signal was amplified and then sent to the envelope detector, which performed frequency down-conversion of the 28 GHz intermediate frequency signal.

The down-converted baseband signal was then sent to the digital storage oscilloscope (DSO) and the ESTT event timer via a custom-made LPF with a bandwidth of up to 1.8 GHz for analysis. This specific LPF (see Chapter 2) was purposefully utilized to broaden the received pulses for accurate detection with the ESTT, as the group delay of this filter remains nearly constant for frequencies up to 3 GHz, thus reducing pulse shape distortions. The pulses after the LPF in the RAU receiver are broadened to approximately 500 ps, facilitating their detection by the ESTT. However, the expansion comes at the cost of the pulse waveform amplitude.

Data Transmission Experiments

The transmitted data were generated as a 1.224×10^6 bit long PRBS using the Mersenne Twister pseudo-random number generator with the order of 623, establishing a minimum detectable BER of 8.17×10^{-7}. The data were saved for later comparison with the demodulated data. The TR-PPM waveforms were generated offline in MATLAB with pulse durations varying from 500 ps to 100 ps and time bin durations ranging from 200 ps to 50 ps, with and without ECC. Error correction was implemented using Gray code alone and Gray code with RS ECC.

Two sets of experiments were performed, with and without a 20 km SMF link, and BER measurements were made with and without ECC. The results are presented in Figs. 3.2 and 3.3.

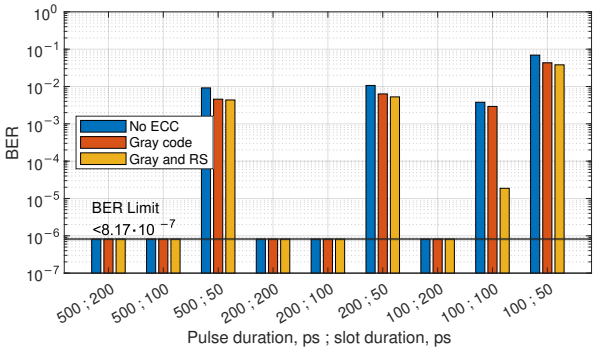


Fig. 3.2. Data transmission experiment results for the B2B connection.

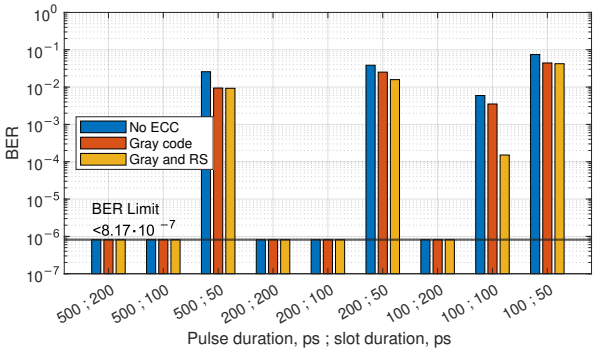


Fig. 3.3. Data transmission experiment results for the connection with 20 km SMF.

All measurements with a time bin duration of 200 ps demonstrate error-free transmission. Error-free transmission was also achieved with both 500 ps and 200 ps pulse durations, using a time bin duration of 100 ps.

It can be seen that the employment of Gray code, which ensures that only one bit is flipped if the received pulse is located in the adjacent time bin, slightly decreases the BER, which is further reduced by the use of RS (255, 223) code. Employment of RS code significantly reduces the BER for measurements with the pulse duration of 100 ps and time bin duration of 100 ps.

For all measurements involving the time bin duration of 50 ps, the impact of the RS code is negligible, which can be attributed to the high amount of flipped bits in the TR-PPM frames that carry the parity bytes.

Comparing measurements with and without the 20 km SMF, the B2B measurements result in a lower overall BER. BER degradation can be attributed to dispersion in the fiber, which causes degradation of the pulse shape and a reduction in the steepness of the rising edge. This, in turn, increases sensitivity to additive noise, resulting in errors in pulse position measurements by the ESTT.

The primary factor influencing the performance of the ARoF TR-PPM communication system is the time bin duration, which directly determines the system's tolerance to jitter. The results validate the effectiveness of the implemented encoding algorithms, as enabling ECC reduces the BER in both the 20 km SMF and B2B setups.

Full description can be seen in [71].

3.2 Design and Evaluation of ISAC-Capable PPM-Based Radar System

This section presents the first implementation of an ARoF-based ISAC-capable radar system utilizing PPM, with a custom-built modulator and a high-precision time tagger, the ESTT 7 Series [158], enabling sub-nanosecond PPM slot durations and transmission over a long SMF span.

Compared to commonly used radar sensing solutions, such as those used in autonomous driving, aerial and ground object monitoring, and weather monitoring [159–162], namely frequency modulated continuous wave (FMCW) and pulse-Doppler radars, both of which offer range and velocity measurement capabilities, the proposed architecture addresses several limitations. FMCW radars are usually quite power-hungry due to continuous transmission and reception and require complex RAUs; meanwhile, pulse-Doppler radars encounter limitations in performing precise absolute range measurements and in detecting slow-moving targets as they rely on Doppler shifts [163, 164]. The proposed architecture achieves precise range measurements by directly measuring the pulse time of arrival (ToA) even for low-velocity or stationary targets. When combined with ARoF, the PPM waveform used mitigates the phase noise accumulation issue in optical FMCW systems [165–167].

A 6.6 GHz pulse radar was implemented due to the extensive super-high-frequency (SHF) infrastructure [168, 169], which can be easily repurposed for ISAC systems. The impact of long SMF spans on the quality of the PPM signal, measured BER, and range accuracy was investigated. Also, the impact of fiber-induced chromatic dispersion compensation in the optical subsystem is evaluated, given that PON systems are intrinsically designed and assessed with dispersion effects accounted for.

Experimental System Description

The experimental system consisted of the central office (CO), where the optical carrier and the RF signals were generated and detected, and the RAU, which radiated and received the RF signal, as shown in Fig. 3.4.

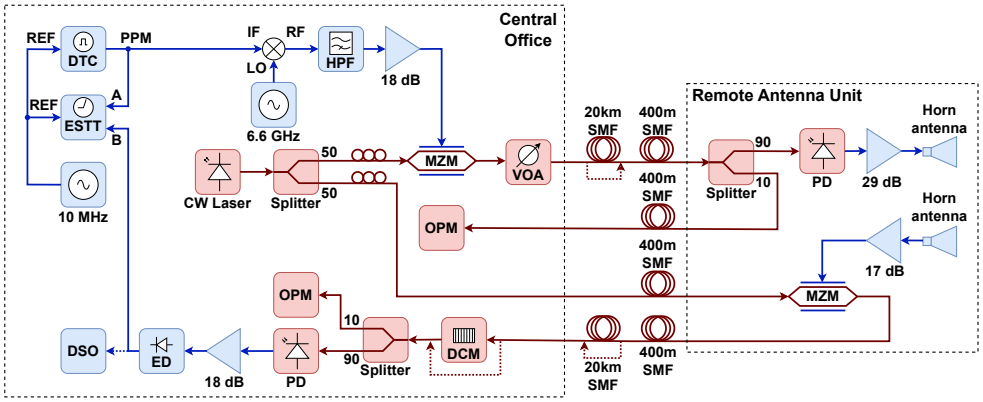


Fig. 3.4. Setup block diagram of the ISAC-capable PPM-based radar system utilizing ARoF.

The transmitted PRBS was generated in MATLAB software, using the 623-order Mersenne Twister pseudo-random number generator. In total, 5.12×10^6 bits were generated, saved as 40 data files, each containing 16000 PPM symbols (one symbol being 8 bits long, therefore the modulation order $M = 256$), and loaded into the modulator control software on the PC.

In the CO, the baseband PPM waveform was generated using the custom-built PPM modulator. The PPM waveform was mixed with the 6.6 GHz RF carrier. The filtered signal was amplified and fed into the RF input port of the MZM. The optical carrier wavelength was 1550 nm, and the laser's optical output power was +12 dBm. The optical output of the MZM was routed to a variable optical attenuator (VOA), which was used to precisely control the optical power incident on the PD in the RAU, maintaining a consistent level of −15 dBm across all connection scenarios. The optical signal was passed to the RAU through a 400 m long SMF span with the option to add an additional 20 km of SMF. In the RAU, the signal was converted to the electrical domain using the PD. The AC-coupled electrical output of the PD was amplified and then radiated by the horn antenna.

On the receiver side, the same type of antenna as in the transmitter was used. The antennas were located next to each other, and the measured isolation between the antennas was 40 dB. The received signal was amplified and fed into the RF input of another MZM, which receives the optical carrier from the CO. The optical output of the MZM was fed into a dispersion compensation module (DCM), which could be bypassed and replaced with a 3 dB optical attenuator. The total dispersion for both 20 km SMF (total 40 km) spools was measured to be 681 ps/nm at 1550 nm. The optical signal was subsequently delivered to the PD, and the resulting electrical signal was amplified and down-converted using a custom-built envelope detector (ED). The re-

ceived and down-converted signal was sent to the "B" input of the ESTT, whereas the "A" input of the ESTT was connected to the modulator to record the time tags of the transmitted pulses, which are necessary for range estimation.

Experimental Parameters

The subframe duration $T_{\text{sf}} = 300$ ns was chosen as such to make sure that, at every tested slot duration Δ, pulses do not arrive within the dead time window of the ESTT. The slot duration range of 10—1000 ps was chosen, as $\Delta = 10$ ps is the shortest possible slot duration that can be generated by the custom-built modulator. The upper limit of slot duration equal to 1000 ps was chosen as it represents the lower end of the typical slot durations used in real-world state-of-the-art PPM data transmission systems, such as those used by National Aeronautics and Space Administration (NASA) and European Space Agency (ESA) [33, 34, 170]. The presented system can achieve an undetectable low error rate at this slot duration.

The maximum bit rate for the given set of constraints ($T_{\text{sf}} = 300$ ns, $T_{\text{break}} = 20$ ms, $N = 16000$) is around 5 Mbit/s, and, as such, the bit rate is acceptable and close to other practically implemented systems [171]. The full list of experimental parameters is shown in Table 3.1.

Table 3.1

Summary of the Main Experimental Parameters

Parameter	Value
Modulation type	PPM
Slot duration Δ	10–1000 ps
Modulation order M	256
Bits per symbol	8
PPM transfer frame size N	16000 symbols
Subframe duration T_{sf}	300 ns
Number of transfer frames sent	40
Total number of bits sent	5.12×10^6
Pulse FWHM τ	2.5 ns
RF carrier frequency	6.6 GHz
Distance to the static reflector	4 m
Optical B2B distance	800 m
Total distance with SMF	40.8 km
Optical carrier wavelength	1550 nm
DCM value	−681 ps/nm

Experimental Configurations

The measurements were conducted with a static metallic reflector located 4 m from the RAU. The data transmission experiments were conducted with and without Gray coding in four system connection configurations:

1) electrical back-to-back (B2B) connection, where the modulator was directly connected to the ESTT via a coaxial cable;
2) optical B2B connection, where the optical transmission network was connected with only the 800 m (400 m each direction) SMF;
3) optical connection with 40 km SMF, where 20 km spools were added in the optical branches that carry the PPM signal in each direction;
4) optical connection with 40 km SMF and DCM.

The range measurements were conducted for all three optical connection scenarios by measuring the ToA of the pulses on both channels of the ESTT and calculating the ToF. The average ToF was calculated over each PPM transfer frame to eliminate relatively large range discrepancies that can be present when considering each transmitted and received pulse individually. The distance d was calculated by knowing the propagation velocity, i.e., the speed of light:

$$d = \frac{(t_\mathrm{m} - t_0)}{2} \cdot c \,, \tag{3.1}$$

where t_m is the measured average time difference between the transmitted and received pulses, t_0 is the propagation delay in the system, and c is the speed of light.

While the ESTT offers picosecond-level timing accuracy that enables centimeter-level range accuracy, its ability to resolve multiple targets is limited by the 40 ns dead time, which corresponds to about 6 m separation between detectable targets. If the dead time of the ESTT were to be eliminated, the range resolution ΔR is limited by the formula $\Delta R = c \cdot \tau/2$, where c is the speed of light and τ is the pulse duration.

Results

The data transmission measurement results without Gray coding are shown in Fig. 3.5 (a), while the results with Gray coding are shown in Fig. 3.5 (b). The estimated BER lower limit is 5.86×10^{-7} at a 95 % confidence level, given the number of bits sent.

As shown in the reported results, in the electrical B2B configuration, zero errors were observed over 5.12×10^6 bits at $\Delta = 100$ ps, meaning the modulator achieved error-free transmission with and without Gray coding, whereas at $\Delta = 50$ ps slot duration, the Gray code significantly reduced the BER. The optical transmission network significantly degraded the BER, achieving error-free transmission only at $\Delta = 500$ ps for the optical B2B case and at $\Delta = 750$ ps for cases with 40 km SMF. In the optical configurations, improvements were observed at $\Delta \geq 750$ ps slot durations. For all cases, when the BER does not approach the established limit, the 95 % confidence interval is less than 6 %.

It can be seen that adding a 40 km SMF span slightly degrades performance compared to the optical B2B connection scenario. The impact is not significant, as the system achieves error-free transmission at $\Delta \geq 750$ ps. This degradation is consistent with the observed edge broadening, where accumulated chromatic dispersion reduced the edge slope and increased jitter, leading to

slightly increased BER in this case.

The results obtained with the 40 km SMF and DCM value of −681 ps/nm, which nominally compensated the accumulated second-order dispersion at the carrier wavelength, show a slight improvement in BER. The performance did not fully return to the level observed in the optical B2B case due to residual higher-order dispersion and practical device limitations.

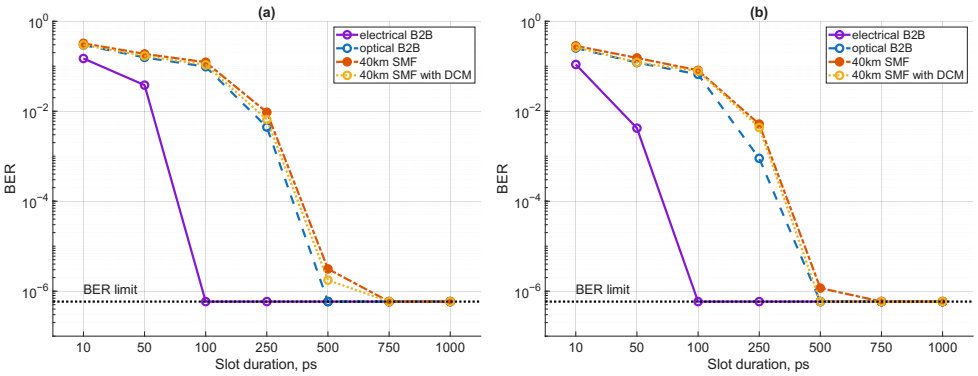


Fig. 3.5. Measured BER as a function of slot duration: (a) without Gray coding, (b) with Gray coding.

As for the range measurements, presented in Table 3.2 and Fig. 3.6, in the optical B2B connection, the absolute range deviation was approximately 0.6741 cm. With the addition of a 40 km SMF, the deviation increased slightly to 0.8610 cm, while incorporating the DCM reduced the deviation to 0.6144 cm, but in this case, the interquartile range was larger. The results are consistent with the previously described considerations and show that dispersion compensation can slightly improve the accuracy. The effect of the dispersion in the SMF is slight, at least in the tested distance, and the main factor impacting the range accuracy is the accuracy of the ESTT and the jitter introduced by other hardware (PD, envelope detector, etc.), as only the measurement of the relative ToA between the transmitted and received pulses is required, which is not impacted by the quality of the generated pulse sequence. Conversely, the jitter present in the transmission system degrades measurement accuracy, and it is not possible to achieve ToF measurement accuracy close to the stated RMS accuracy of the ESTT of about 1.5 ps.

The presented architecture shows improved accuracy compared to existing, more complex and costly solutions [172–174]; on the other hand, newer experimental terahertz systems report sub-micron accuracy [175] using interferometric ToF.

The broader and slightly shallower pulse rising edge, which results from the dispersion in the SMF, impacts the BER and range accuracy measurements as the ESTT triggers at a set threshold voltage; therefore, additive noise in the pulse waveform may cause the triggering event to happen at a time, which is slightly before or after the expected time.

Table 3.2

Range Measurement Results

Connection	Mean range, m	Absolute deviation, cm	Standard deviation, cm	Interquartile range, cm
Optical B2B	4.0198	0.6741	0.1803	0.2789
40 km SMF	4.0189	0.8610	0.2405	0.3657
40 km SMF with DCM	4.0188	0.6144	0.1858	0.3330

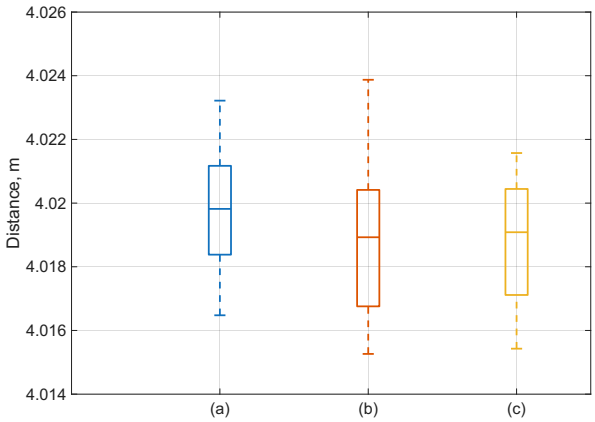


Fig. 3.6. Range measurement errorbar plot: (a) optical B2B connection, (b) optical connection with 40 km SMF, (c) optical connection with 40 km SMF and DCM.

In summary, using the optical transmission network, error-free transmission was achieved at a slot duration of 500 ps, and with an additional 40 km of SMF, at 750 ps. The system outperforms existing solutions in both BER and the minimum usable slot duration, and is ISAC-capable. Gray coding reduced the resulting BER, making it effective for PPM data transmission.

The range measurement accuracy was 0.6741 cm in the optical B2B case and increased slightly to 0.8610 cm in the case with a 40 km SMF. The effect of dispersion compensation was tested and found to reduce the BER and to slightly increase the range accuracy. The improvement is slight and may not justify the added complexity and cost. The range accuracy achieved with the time tagger significantly outperforms that of widely used radar systems, and enables accurate range and velocity estimation with a lower power budget than an FMCW radar, without depending on Doppler-induced frequency shifts. The main limitation of the range resolution, currently 6 m for multi-target scenarios, is the dead time of the TDC. While the pulse duration does not carry information in PPM, reducing it is important for energy efficiency and range resolution in ISAC, given that the TDC dead time is kept low.

Full description can be seen in [72].

3.3 Summary of the Third Thesis

The third thesis was devoted to proving that in optical PPM-based ISAC systems, a BER below 1×10^{-6} along with a sensing accuracy below 5 cm at a range of at least 4 m with optical transmission distance exceeding 40 km can be achieved by using high-order PPM and a time tagger for SLR applications as the receiver. ARoF-based communication system using PPM was developed and tested with 20 km of SMF and 5 m 28 GHz RF link, using pulses as short as 100 ps. The experimental validation proved that the PPM waveform is highly resilient to distortions introduced by the transmission network, achieving BER values as low as 8.17×10^{-7}. This system was used as a testbed to develop a PPM-based ISAC pulse radar system, employing a time-tagger as the receiver. For the first time, joint radar sensing and communications using a 6.6 GHz PPM-based system with up to 40 km of SMF was experimentally demonstrated. The experimental results using 10–1000 ps slot durations, PPM order of 256, and a subframe duration of 300 ns achieved BER values as low as 5.86×10^{-7} at a 95 % confidence level, with and without Gray coding. In the distance measurements, absolute deviation below 0.861 cm was observed. The data transmission and distance measurement test results significantly exceeded the target set out in this thesis, therefore proving it. Additionally, the impact of chromatic dispersion on the PPM waveform was explored and found not to significantly affect the BER and range accuracy.

Full description containing the results presented in this Chapter can be seen in [71] and [72].

CONCLUSIONS

The Thesis is written as a summary of thematically unified scientific publications and is devoted to the design, implementation, and experimental validation of PPM-based communication systems, with the main objective being to design, develop, and test a PPM-based ISAC-capable joint radar and communication system utilizing ARoF technology and a custom-built PPM modulator with a commercial time-tagger as the demodulator, which can serve as a testbed for future UWB sensing, as well as space communication research. The main results and findings of the Thesis are as follows:

1. An experimental testbed and an AWG-based setup have been developed to explore PPM signal detection with a high-precision time-tagger for SLR applications. It was shown that additive noise on the PPM waveform can significantly impact the BER in time-tagger-based systems because the detection threshold level is fixed, potentially causing a false time tag in a neighboring time slot. Nevertheless, it was demonstrated that a time-tagger is a robust and highly precise means for PPM signal demodulation under the test conditions.
2. Two programmable digital delay line-based PPM modulators have been developed and experimentally validated. The tests indicate stable PPM sequence generation with RMS jitter as low as 7.65 ps. The most recently developed modulator is capable of generating a 16000-symbol-long PPM sequence with slot duration as low as 10 ps and reconfigurable modulation order. The concept of a DDL-based modulator was verified and proven to be an excellent, highly stable means of PPM signal generation in subsequent experiments.
3. The jitter distribution was analyzed and found to be distributed approximately normally, thereby enabling the use of ECC algorithms. The systematic errors, including clock drift and synchronization between the transmitter and receiver, were analyzed. It was found that the clock drift manifests as a constant offset from the expected pulse positions in the PPM sequence, while synchronization errors provide for a constantly increasing offset. Techniques such as a synchronization preamble in the pulse sequence can be used to mitigate these issues.
4. It was found that Gray coding provides for the most significant decrease in BER, as the code allows for one bit error to occur when the pulse is received in the neighboring time slot, which is the most common cause of errors. RS code was proposed to correct bit errors in the transmitted data, and simulations show that it provided the most benefit in the cases when clock drift error is present.
5. Electrical and optical pulse expansion techniques were proposed, as the time-tagger has a minimum required pulse duration. The experimental results demonstrate that a pulse can be expanded electrically using an LPF, and optically using an FBG to 2–3 times its original duration while preserving the waveform shape for stable detection

using the time-tagger.

6. An ARoF-based PPM communication system was designed and experimentally validated, achieving BER values as low as 8.17×10^{-7} using 200 ps slot duration using 20 km long SMF span and a 5 m RF link. It was shown that nonlinear optical effects (NOE) do not significantly affect the PPM waveform and validates PPM as an efficient and robust means for data transmission in optical communication systems.
7. An ISAC-capable ARoF-based 6.6 GHz joint radar and communication system was developed and experimentally validated. The system achieved BER values as low as 5.86×10^{-7} at a 95 % confidence level, with and without Gray coding, and absolute range measurement deviation below 0.861 cm, using a total SMF distance of 40 km and a 4 m distance to the target. The main contributing success factor was the use of the high-precision time-tagger, which was experimentally demonstrated for the first time in this Thesis; however, the dead time of the time-tagger significantly limits the range resolution of such a system.
8. The impact of chromatic dispersion was evaluated by using a tunable DCM and found to be insignificant at least in the tested SMF span distances. While dispersion compensation slightly decreased BER and improved range accuracy, the slight effects do not outweigh the added cost and complexity.

The main results presented in this Thesis have been published in three peer-reviewed international journals ranking in the top 25th percentile (Q1) by citation index, as well as four peer-reviewed international conference proceedings.

The findings of this Thesis are an important contribution to the field of UWB-based ISAC-capable systems and can be extended to the field of deep space communications, which increasingly relies on time-tagging technology and PPM for long-range, robust, energy-efficient data links. In future applications, the dead time of the time-tagger (40 ns in the case of ESTT) must be decreased, as this is the main limiting factor of the range resolution (around 6 m in the presented research). Also, as attention is paid to higher throughput of such communication systems, significant software limitations must be resolved, as the break between the transfer frames significantly limits the achievable real-world data rate, even though the developed modulator is capable of multi-gigabit-per-second data transfer rates at the hardware level.

REFERENCES

[1] Yang, L., and Giannakis, G. "Ultra-wideband communications: an idea whose time has come." *IEEE Signal Processing Magazine* 21.6 (2004), pp. 26–54. DOI: 10.1109/MSP.2004.1359140.

[2] Yajnanarayana, V., and Handel, P. "Joint Estimation of TOA and PPM Symbols Using Sub-Nyquist Sampled IR-UWB Signal." *IEEE Communications Letters* 21.4 (Apr. 2017), pp. 949–952. ISSN: 1089-7798. DOI: 10.1109/LCOMM.2017.2650231.

[3] Jajodia, B., Mahanta, A., and Ahamed, S. R. "IEEE 802.15.6 WBAN Standard Compliant IR-UWB Time-Hopping PPM Transmitter using SRRC signaling pulse." *AEU – International Journal of Electronics and Communications* 117 (Apr. 2020), p. 153119. ISSN: 1434-8411. DOI: 10.1016/J.AEUE.2020.153119.

[4] Youssef, A. A. "Adaptive LDPC coded high data rate based IR-UWB combined with VMIMO system for vehicular communication links." *AEU – International Journal of Electronics and Communications* 169 (Sept. 2023), p. 154747. ISSN: 16180399. DOI: 10.1016/j.aeue.2023.154747.

[5] Somov, A., and Baraev, A. "Consist-to-Consist communications in the trains: Is it time to use ultra wide-band?" *Computers & Electrical Engineering* 72 (Nov. 2018), pp. 965–975. ISSN: 0045-7906. DOI: 10.1016/J.COMPELECENG.2018.02.023.

[6] Salmento, M. L. G. et al. "An enhanced receiver for an impulsive UWB-based PLC system for low-bit rate applications." *Digital Signal Processing* 70 (Nov. 2017), pp. 145–154. ISSN: 1051-2004. DOI: 10.1016/J.DSP.2017.08.003.

[7] Duan, S. et al. "Ultra-Wideband Radio Channel Characteristics for Near-Ground Swarm Robots Communication." *IEEE Transactions on Wireless Communications* 19.7 (July 2020), pp. 4715–4726. ISSN: 1536-1276. DOI: 10.1109/TWC.2020.2986446.

[8] Rendevski, N., and Cassioli, D. "Potentials of low-complexity Rake receivers for 60 GHz UWB wireless communication systems." *2015 IEEE 1st International Forum on Research and Technologies for Society and Industry, RTSI 2015 – Proceedings* (2015), pp. 94–99. DOI: 10.1109/RTSI.2015.7325077.

[9] Ghavami, M., Michael, L. B., and Kohno, R. *Ultra Wideband Signals and Systems in Communication Engineering*. John Wiley & Sons, Ltd, 2004. DOI: 10.1002/0470867531.

[10] Nguyen, C., and Miao, M. *Design of CMOS RFIC Ultra-Wideband Impulse Transmitters and Receivers*. Springer International Publishing, 2017. DOI: 10.1007/978-3-319-53107-6.

[11] Chandrakasan, A. P. et al. “Low-Power Impulse UWB Architectures and Circuits.” *Proceedings of the IEEE* 97.2 (Feb. 2009), pp. 332–352. DOI: 10.1109/jproc.2008.2008787.

[12] Black, H. S. et al. “A Multichannel Microwave Radio Relay System.” *Transactions of the American Institute of Electrical Engineers* 65.12 (Dec. 1946), pp. 798–806. DOI: 10.1109/t-aiee.1946.5059251.

[13] Mahdiraji, G. A., and Zahedi, E. “Comparison of Selected Digital Modulation Schemes (OOK, PPM and DPIM) for Wireless Optical Communications.” *2006 4th Student Conference on Research and Development*. June 2006, pp. 5–10. DOI: 10.1109/SCORED.2006.4339297.

[14] Barnwell, N. et al. “The miniature optical communication transceiver-A compact, power-efficient lasercom system for deep space nanosatellites.” *Aerospace* 6.1 (2019). ISSN: 22264310. DOI: 10.3390/aerospace6010002.

[15] Elganimi, T. Y. “Studying the BER performance, power- and bandwidth- efficiency for FSO communication systems under various modulation schemes.” *2013 IEEE Jordan Conference on Applied Electrical Engineering and Computing Technologies, AEECT 2013. IEEE Computer Society.* (2013). DOI: 10.1109/AEECT.2013.6716426.

[16] Cui, S., Goldsmith, A., and Bahai, A. “Energy-Efficiency of MIMO and Cooperative MIMO Techniques in Sensor Networks.” *IEEE Journal on Selected Areas in Communications* 22.6 (Aug. 2004), pp. 1089–1098. DOI: 10.1109/jsac.2004.830916.

[17] Hamkins, J. *Pulse Position Modulation*. Nov. 2007. DOI: 10.1002/9781118256053.ch32.

[18] Dai, L. et al. “Research on the Pulse-position Modulation in the Digital Communication System.” *2021 International Conference on Wireless Communications and Smart Grid (ICWCSG)*. 2021, pp. 8–12. DOI: 10.1109/ICWCSG53609.2021.00009.

[19] Huan, L. “Simulation on the design of digital pulse position modulation system.” *International Conference on Neural Networks, Information, and Communication Engineering (NNICE 2022)*. Ed. by Tiwari, R. SPIE, July 2022. DOI: 10.1117/12.2640677.

[20] Proakis, J., and Salehi, M. *Digital Communications, 5th edition*. McGraw-Hill Higher Education, 2008.

[21] Karp, S., and Gagliardi, R. “The Design of a Pulse-Position Modulated Optical Communication System.” *IEEE Transactions on Communications* 17.6 (Dec. 1969), pp. 670–676. DOI: 10.1109/tcom.1969.1090162.

[22] Jing, M., Li-ying, T., and Siyuan, Y. “Technologies and applications of free-space optical communication and space optical information network.” *Journal of communications and information networks* (June 2016). DOI: 10.11959/j.issn.2096-1081.2016.005.

[23] Wilson, B., and Ghassemlooy, Z. “Pulse time modulation techniques for optical communications: a review.” *IEE Proceedings J Optoelectronics* 140.6 (1993), p. 346. DOI: 10.1049/ip-j.1993.0055.

[24] Saeed, R. et al. “Ultra Wide Band (UWB) Ad-hoc Networks: Review and Trends.” *Journal of Computer Science* 1.1 (Jan. 2005), pp. 35–39. DOI: 10.3844/jcssp.2005.35.39.

[25] *Pulse Position Modulation : Block Diagram, Circuit, Working, Generation with PWM & Its Applications*. URL: https://www.elprocus.com/pulse-position-modulation/.

[26] Green, R. J. “Comparison of pulse position modulation and pulse width modulation for application in optical communications.” *Optical Engineering* 46.6 (June 2007), p. 065001. DOI: 10.1117/1.2746010.

[27] Ai-ping, H. et al. “A differential pulse position width modulation for optical wireless communication.” *2009 4th IEEE Conference on Industrial Electronics and Applications*. 2009, pp. 1773–1776. DOI: 10.1109/ICIEA.2009.5138501.

[28] Sacko, D., and Kéïta, A. A. “Techniques of Modulation: Pulse Amplitude Modulation, Pulse Width Modulation, Pulse Position Modulation.” *IJEAT* 7.2 (Dec. 2017), p. 9. URL: https://www.ijeat.org/wp-content/uploads/papers/v7i2/B5251127217.pdf.

[29] Jahid, A., Alsharif, M. H., and Hall, T. J. “A contemporary survey on free space optical communication: Potentials, technical challenges, recent advances and research direction.” *Journal of Network and Computer Applications* 200 (Apr. 2022), p. 103311. DOI: 10.1016/j.jnca.2021.103311.

[30] Fu, X. et al. “Research and Simulation of PPM Modulation and Demodulation System on Spatial Wireless Optical Communication.” *2010 Symposium on Photonics and Optoelectronics*. IEEE, June 2010. DOI: 10.1109/sopo.2010.5504142.

[31] Tang, W. et al. “The Research Process, Application, and the Future Development of Pulse-Position Modulation.” *Journal of Physics: Conference Series* 2384.1 (Dec. 2022), p. 012026. DOI: 10.1088/1742-6596/2384/1/012026.

[32] Wang, Y. et al. “Research on PPM Modulation Performance of Deep Space Optical Communication.” *2021 International Conference on Electronic Information Engineering and Computer Science (EIECS)*. 2021, pp. 5–8. DOI: 10.1109/EIECS53707.2021.9588043.

[33] Simon, W. P. et al. “Field-Programmable Gate Array Implementation of a Single Photon-Counting Receive Modem.” *Free-Space Laser Communications XXXVI*. Ed. by Hemmati, H., and Robinson, B. S. San Francisco, United States: SPIE, Mar. 2024, p. 58. DOI: 10.1117/12.3001097.

[34] Jhaidri, M.-A. et al. “Implementation of High-Photon-Efficiency Optical Modem for ESA’s Technology Demonstration of Deep-Space Optical Communication with the NASA Psyche Spacecraft.” *International Conference on Space Optics – ICSO 2024*. Antibes Juan-les-Pins, France: SPIE, July 2025, p. 211. DOI: 10.1117/12.3075346.

[35] Sodnik, Z., Furch, B., and Lutz, H. “Free-space laser communication activities in Europe: SILEX and beyond.” *Conference Proceedings – Lasers and Electro-Optics Society Annual Meeting-LEOS (pp. 78–79)*. (2006). DOI: 10.1109/LEOS.2006.278845.

[36] Cryan, R. A., and Unwin., R. T. “Optical Employing Space Communications Pulse Position Modulation.” *IEE Colloquium on Advanced Modulation and Coding Techniques for Satellite Communications*. (1992).

[37] Guelman, M. et al. “Acquisition and Pointing Control for Inter-Satellite Laser Communications.” *IEEE Transactions on Aerospace and Electronic Systems* 40.4 (Oct. 2004), pp. 1239–1248. ISSN: 1557-9603. DOI: 10.1109/TAES.2004.1386877.

[38] Al Zaman, A., and Islam, N. “Modulation Schemes and Pulse Shaping in Ultra-Wideband.” *IEEE SoutheastCon 2008*. Apr. 2008, pp. 142–146. DOI: 10.1109/SECON.2008.4494274.

[39] Huo, X. et al. “C-Band 200 Gbit/s/λ PS-PAM-8 Transmission Over 2-km SSMF for Optical Interconnections.” *IEEE Photonics Journal* 16.3 (2024), pp. 1–7. DOI: 10.1109/JPHOT.2024.3381232.

[40] Pan, S., and Yao, J. “UWB-Over-Fiber Communications: Modulation and Transmission.” *Journal of Lightwave Technology* 28.16 (2010), pp. 2445–2455. DOI: 10.1109/JLT.2010.2043713.

[41] Pan, S., and Yao, J. “Performance evaluation of UWB signal transmission over optical fiber.” *IEEE Journal on Selected Areas in Communications* 28.6 (2010), pp. 889–900. DOI: 10.1109/JSAC.2010.100813.

[42] Abraha, S. T. et al. “Performance Evaluation of IR-UWB in Short-Range Fiber Communication Using Linear Combination of Monocycles.” *Journal of Lightwave Technology* 29.8 (2011), pp. 1143–1151. DOI: 10.1109/JLT.2011.2120595.

[43] Edwards, B. L. “Latest Status of the CCSDS Optical Communications Working Group.” *2022 IEEE International Conference on Space Optical Systems and Applications, ICSOS 2022*. IEEE, Mar. 2022, pp. 1–6. ISBN: 9781665434393. DOI: 10.1109/ICSOS53063.2022.9749734.

[44] Kim, M.-J. et al. “Performance Analysis and Implementation of Biased MC-PPM for Optical Energy Transfer and Communication System.” *Physical Communication* 71 (Aug. 2025), p. 102684. ISSN: 1874-4907. DOI: 10.1016/j.phycom.2025.102684.

[45] Huang, J. et al. “Real-Time and High-Speed Underwater Photon-Counting Communication Based on SPAD and PPM Symbol Synchronization.” *IEEE Photonics Journal* 13.5 (Oct. 2021), pp. 1–9. ISSN: 1943-0655. DOI: 10.1109/JPHOT.2021.3113659.

[46] Kaszubowska-Anandarajah, A. et al. “An IR-UWB Photonic Distribution System.” *IEEE Photonics Technology Letters* 20.22 (Nov. 2008), pp. 1884–1886. ISSN: 1941-0174. DOI: 10.1109/LPT.2008.2004989.

[47] Fujiwara, Y. “Self-Synchronizing Pulse Position Modulation With Error Tolerance.” *IEEE Transactions on Information Theory* 59.9 (Sept. 2013), pp. 5352–5362. ISSN: 1557-9654. DOI: 10.1109/TIT.2013.2262094.

[48] Mietzner, J., and Lampe, L. “Nested PPM for Visible Light Communication With Heterogeneous Optical Receivers.” *IEEE Photonics Journal* 16.4 (2024), pp. 1–12. DOI: 10.1109/JPHOT.2024.3406156.

[49] Dix-Matthews, B. P. et al. “Ultra-Wideband Free-Space Optical Phase Stabilization.” *IEEE Communications Letters* 25.5 (May 2021), pp. 1610–1614. ISSN: 1089-7798. DOI: 10.1109/LCOMM.2021.3053943.

[50] Landolsi, T., and Elrefaie, A. F. “Effects of pointing errors and channel fading on the performance of free-space optically-preamplified PPM systems.” *International Journal of Communication Systems* 29.15 (Oct. 2016), pp. 2313–2324. ISSN: 1074-5351. DOI: 10.1002/dac.3166.

[51] Wen, Y. et al. “Free Space Optical Integrated Sensing and Communication Based on LFM and CPM.” *IEEE Communications Letters* 28.1 (Jan. 2023), pp. 43–47. ISSN: 15582558. DOI: 10.1109/LCOMM.2023.3332658.

[52] Qaisar, M. U. F. et al. “The Role of ISAC in 6G Networks: Enabling Next-Generation Wireless Systems.” *IEEE Transactions on Network Science and Engineering* 13 (2026), pp. 7825–7861. DOI: 10.1109/TNSE.2026.3666665.

[53] Perez Santacruz, J. “Analog Radio-over-Fiber for 5G/6G Millimeter-Wave Communications.” Ph. D. Thesis. Eindhoven University of Technology, 2022.

[54] Singh, G. et al. “Toward 6G-V2X: Aggregated RF-VLC for Ultra-Reliable and Low-Latency Autonomous Driving.” *IEEE Communications Standards Magazine* 8.4 (2024), pp. 80–87. DOI: 10.1109/MCOMSTD.0001.2300005.

[55] Colson, S., and Hoff, H. “Ultra-Wideband Technology for Defence Applications.” *2005 IEEE International Conference on Ultra-Wideband*. Sept. 2005, pp. 615–620. DOI: 10.1109/ICU.2005.1570059.

[56] Kaushik, A. et al. “Integrated Sensing and Communications for IoT: Synergies with Key 6G Technology Enablers.” *IEEE Internet of Things Magazine* 7.5 (2024), pp. 136–143. DOI: 10.1109/IOTM.001.2400052.

[57] Campbell, S. P. *Integrated Sensing and Communications (ISAC) Report*. Tech. rep. Findings from the National ISAC Workshop, April 9–10, 2025. George Mason University, Office of Research, Innovation, and Economic Impact, May 2025. URL: https://rt.cto.mil/wp-content/uploads/2025/07/ISAC-Report-from-Apr-2025-Workshop.pdf.

[58] Liu, F. et al. “ISAC With UWB: Reliable Decoupling and Target Sensing.” *IEEE Transactions on Wireless Communications* 23.11 (2024), pp. 15957–15972. DOI: 10.1109/TWC.2024.3435070.

[59] Wang, X. et al. “Fundamental Limits on Joint Delay and Doppler Characterization in UWB ISAC Systems.” *2023 IEEE 98th Vehicular Technology Conference (VTC2023-Fall)*. 2023, pp. 1–6. DOI: 10.1109/VTC2023-Fall60731.2023.10333549.

[60] Cai, S. et al. “Pulse-Based ISAC: Data Recovery and Ranging Estimation for Multi-Path Fading Channels.” *IEEE Transactions on Communications* 71.8 (2023), pp. 4819–4838. DOI: 10.1109/TCOMM.2023.3277039.

[61] Yu, M. et al. “FPGA-Based Dual-Pulse Anti-Interference Lidar System Using Digital Chaotic Pulse Position Modulation.” *IEEE Photonics Technology Letters* 33.15 (2021), pp. 757–760. DOI: 10.1109/LPT.2021.3093109.

[62] Yeo, J. et al. “A Flash LiDAR with SA-Based Pulse Position Modulation for Multi-user Interference Cancellation.” *2025 IEEE International Symposium on Circuits and Systems (ISCAS)*. 2025, pp. 1–5. DOI: 10.1109/ISCAS56072.2025.11044208.

[63] Alabd, M. B. et al. “Modified Pulse Position Modulation for Joint Radar Communication Based on Chirp Sequence.” *IEEE Microwave and Wireless Components Letters* 32.10 (2022), pp. 1247–1250. DOI: 10.1109/LMWC.2022.3169287.

[64] Shi, X. et al. “BER Performance Analysis of Non-Coherent Q-Ary Pulse Position Modulation Receivers on AWGN Channel.” *Sensors* 21.18 (2021). DOI: 10.3390/s21186102.

[65] Pulkkinen, M. et al. “45.2% Energy efficiency improvement of UWB IR Tx by use of differential PPM in 180nm CMOS.” *2016 IEEE International Symposium on Circuits and Systems (ISCAS)*. 2016, pp. 193–196. DOI: 10.1109/ISCAS.2016.7527203.

[66] Migla, S. et al. “A Design of UWB Communication Testbed with Event Timer-based PPM Demodulator.” *2022 IEEE 2nd Ukrainian Microwave Week (UkrMW)*. 2022, pp. 691–694. DOI: 10.1109/UkrMW58013.2022.10037100.

[67] Selis, O. et al. “Demonstration of 50 ps Per-Position Differential Pulse Position Modulation Data Transmission.” *2023 IEEE 10th Jubilee Workshop on Advances in Information, Electronic and Electrical Engineering (AIEEE)*. 2023, pp. 1–4. DOI: 10.1109/AIEEE58915.2023.10134802.

[68] Sics, P. E. et al. “Implementation of Reconfigurable 149Mbps TDC-Based PPM Transceiver.” *2024 Joint European Conference on Networks and Communications & 6G Summit (EuCNC/6G Summit)*. 2024, pp. 706–710. DOI: 10.1109/EuCNC/6GSummit60053.2024.10597124.

[69] Migla, S. et al. “Error Analysis and Correction Techniques for PPM Communication Links with Jitter and Clock Drift.” *2024 IEEE International Conference on Microwaves, Communications, Antennas, Biomedical Engineering and Electronic Systems (COMCAS)*. 2024, pp. 1–4. DOI: 10.1109/COMCAS58210.2024.10666259.

[70] Aboltins, A. et al. “Passive Electrical and Optical Methods of Ultra-Short Pulse Expansion for Event Timer-Based TDC in PPM Receiver.” *Electronics* 12.22 (2023). DOI: 10.3390/electronics12224634.

[71] Migla, S. et al. “Ultra-Wideband Analog Radio-over-Fiber Communication System Employing Pulse-Position Modulation.” *Applied Sciences* 15.8 (2025). DOI: 10.3390/app15084222.

[72] Migla, S. et al. “Demonstration of Integrated Sensing and Communications in an ARoF-Based Radar System Utilizing Pulse Position Modulation.” *IEEE Access* 14 (2026), pp. 76251–76264. DOI: 10.1109/ACCESS.2026.3693952.

[73] Li, L., and Townsend, J. K. “M-Ary PPM for Transmitted Reference Ultra-Wideband Communications.” *IEEE Transactions on Communications* 58.7 (July 2010), pp. 1912–1917. ISSN: 1558-0857. DOI: 10.1109/TCOMM.2010.07.080675.

[74] Luo, X., and Giannakis, G. B. “Achievable rates of transmitted-reference ultra-wideband radio with PPM.” *IEEE Transactions on Communications* 54 (9 Sept. 2006), pp. 1536–1541. ISSN: 00906778. DOI: 10.1109/TCOMM.2006.881203.

[75] Aliaberi, A., Sofotasios, P. C., and Muhaidat, S. “Modulation Schemes for Visible Light Communications.” *2019 International Conference on Advanced Communication Technologies and Networking (CommNet)*. Apr. 2019, pp. 1–10. DOI: 10.1109/COMMNET.2019.8742376.

[76] Dahri, F. A., Ali, S., and Jawaid, M. M. “A Review of Modulation Schemes for Visible Light Communication.” *IJCSNS International Journal of Computer Science and Network Security* 18.2 (2018), pp. 117–125.

[77] *Optical communications coding and synchronization*. 1st ed. Recommended Standard CCSDS 142.0-B-1. Consultative Committee for Space Data Systems. Washington, DC, USA, Aug. 2019. URL: https://ccsds.org/Pubs/142x0b1.pdf.

[78] Urkowitz, H. “Energy detection of unknown deterministic signals.” *Proceedings of the IEEE* 55.4 (1967), pp. 523–531. DOI: 10.1109/proc.1967.5573.

[79] Dillard, G. “Pulse-Position Modulation Based on Energy Detection.” *IEEE Transactions on Aerospace and Electronic Systems* AES-9.4 (July 1973), pp. 499–503. DOI: 10.1109/taes.1973.309631.

[80] Durisi, G., and Benedetto, S. “Comparison between coherent and noncoherent receivers for UWB communications.” *Eurasip Journal on Applied Signal Processing* 2005.3 (2005), pp. 359–368. ISSN: 11108657. DOI: 10.1155/ASP.2005.359.

[81] Hussein, S. S., youssif, A., and M., G. H. H. “Performance Analysis and Evaluation of TH-PPM and TH-BPSK under Dynamic Channel Environment.” *International Journal of Future Computer and Communication* (2012), pp. 352–355. ISSN: 20103751. DOI: 10.7763/IJFCC.2012.V1.94.

[82] Khani, H. “Improved Detection Schemes for Non-coherent Pulse-Position Modulation.” *Wireless Personal Communications* 131.3 (Aug. 2023), pp. 2173–2192. ISSN: 0929-6212. DOI: 10.1007/s11277-023-10537-7.

[83] Cassioli, D. et al. “Low Complexity Rake Receivers in Ultra-Wideband Channels.” *IEEE Transactions on Wireless Communications* 6.4 (Apr. 2007), pp. 1265–1275. ISSN: 1536-1276. DOI: 10.1109/TWC.2007.348323.

[84] Zheng, Y. et al. “A 0.18 um CMOS Dual-Band UWB Transceiver.” *2007 IEEE International Solid-State Circuits Conference. Digest of Technical Papers*. IEEE, Feb. 2007, pp. 114–590. ISBN: 1-4244-0852-0. DOI: 10.1109/ISSCC.2007.373614.

[85] Munirathinam, R. et al. “Chaotic Non-Coherent Pulse Position Modulation Based Ultra-Wideband Communication System.” *2021 IEEE Microwave Theory and Techniques in Wireless Communications (MTTW)*. IEEE, 2021, pp. 52–57. DOI: 10.1109/mttw53539.2021.9607075.

[86] Lee, F., and Chandrakasan, A. “A 2.5nJ/b 0.65V 3-to-5GHz Sub banded UWB Receiver in 90nm CMOS.” *Int. Solid State Circuits Conference (ISSCC 07)*. 2007, pp. 116–117.

[87] Shariat, M. et al. “Comparison Between Several Methods of PPM Demodulation Based on Iterative Techniques.” *Telecommunications and Networking – ICT 2004*. Springer Berlin Heidelberg, 2004, pp. 554–559. DOI: 10.1007/978-3-540-27824-5_75.

[88] Sushchik, M. et al. “Chaotic pulse position modulation: a robust method of communicating with chaos.” *IEEE Communications Letters* 4.4 (Apr. 2000), pp. 128–130. DOI: 10.1109/4234.841319.

[89] Wang, W. et al. “Under-Sampling of PPM-UWB Communication Signals Based on CS and AIC.” *Circuits, Systems, and Signal Processing* 34.11 (Nov. 2015), pp. 3595–3609. ISSN: 0278-081X. DOI: 10.1007/s00034-015-0026-4.

[90] Kalisz, J. “Review of methods for time interval measurements with picosecond resolution.” *Metrologia* 41.1 (Dec. 2003), pp. 17–32. DOI: 10.1088/0026-1394/41/1/004.

[91] Mahjoubfar, A. et al. “Time stretch and its applications.” *Nature Photonics* 11.6 (June 2017), pp. 341–351. DOI: 10.1038/nphoton.2017.76.

[92] Jonass, J., Bespal’ko, V., and Lapkovskis, V. “Precision Time Meters for Ground and Space Applications.” *Space-Based Lidar Remote Sensing Techniques and Emerging Technologies*. Cham: Springer Nature Switzerland, 2024, pp. 309–318. DOI: 10.1007/978-3-031-53618-2_27.

[93] Steindorfer, M. A. et al. “Space Debris and Satellite Laser Ranging Combined Using a Megahertz System.” *Nature Communications* 16.1 (Jan. 2025), p. 575. ISSN: 2041-1723. DOI: 10.1038/s41467-024-55777-8.

[94] Piedra, M. A. S. et al. “First Results from the Newly Modernized San Fernando Laser Station: Commemorating 45 Years of Service.” *9th European Conference on Space Debris*. Vol. 9. Bonn, Germany, ESA Space Debris Office, Apr. 2025.

[95] Merz, R., Botteron, C., and Farine, P.-A. “A novel low complexity data demodulation algorithm for pulse position modulation.” *Digital Signal Processing* 22.3 (May 2012), pp. 535–543. DOI: 10.1016/j.dsp.2011.08.008.

[96] Kim, J., and Clerckx, B. “Wireless Information and Power Transfer for IoT: Pulse Position Modulation, Integrated Receiver, and Experimental Validation.” *IEEE Internet of Things Journal* 9.14 (July 2022), pp. 12378–12394. DOI: 10.1109/jiot.2021.3135712.

[97] ScioSense B.V. *Datasheet of TDC-GPX2*. 2018. URL: https://www.sciosense.com/wp-content/uploads/documents/TDC-GPX2-Datasheet.pdf.

[98] Mezerins, A., and Bespal’ko, V. “Estimation of analog-to-time and time-to-digital conversion efficiency in analog optical communication system testbed.” *Proceedings – 2015 Advances in Wireless and Optical Communications, RTUWO 2015*. IEEE, Nov. 2015, pp. 211–214. ISBN: 9781467374316. DOI: 10.1109/RTUWO.2015.7365754.

[99] Solovjova, T. et al. “Picosecond Pulse Expansion Using The Low-Pass Filter in Event Timer-Based PPM Communication System.” *Proceedings of 2022 Workshop on Microwave Theory and Techniques in Wireless Communications, MTTW 2022*. IEEE, Oct. 2022, pp. 29–34. DOI: 10.1109/MTTW56973.2022.9942566.

[100] Hamil, H. et al. “Design and FPGA real-time implementation of PWM and PPM modulation for Ultra Wide Band applications.” *2019 6th International Conference on Image and Signal Processing and their Applications (ISPA)*. 2019, pp. 1–5. DOI: 10.1109/ISPA48434.2019.8966916.

[101] Roche, R. J. et al. “Reconfigurable, intelligently-adaptive, communication system, an SDR platform.” *34th AIAA International Communications Satellite Systems Conference, 2016*. 2016. ISBN: 9781624104572. DOI: 10.2514/6.2016-5718.

[102] Schlemmer, H. et al. “Results from a CCSDS-compliant High Photon Efficiency Downlink SDR Platform.” *2019 8th International Workshop on Tracking, Telemetry and Command Systems for Space Applications (TTC)*. IEEE, Sept. 2019, pp. 1–5. ISBN: 978-1-7281-3700-1. DOI: 10.1109/TTC.2019.8895458.

[103] *Optical communications physical layer*. 1st ed. Recommended Standard CCSDS 141.0-B-1. Consultative Committee for Space Data Systems. Washington, DC, USA, Aug. 2019. URL: https://ccsds.org/Pubs/141x0b1.pdf.

[104] Spolitis, S. et al. “Demonstration of 512-TR-PPM Fiber Optical Transmission Link.” *2023 Photonics & Electromagnetics Research Symposium (PIERS)*. 2023, pp. 1416–1422. DOI: 10.1109/PIERS59004.2023.10221307.

[105] Sics, P. E. et al. “Programmable Delay Line Based High-speed PPM Modulator with 50 ps Time Resolution.” *2023 Photonics & Electromagnetics Research Symposium (PIERS)*. 2023, pp. 1779–1786. DOI: 10.1109/PIERS59004.2023.10221245.

[106] Barrett, T. W. “History of Ultra Wideband Communications and Radar: Part I, UWB Communications.” *Microwave Journal* (Jan. 2001), pp. 22–56.

[107] Barrett, T. W. “History of Ultra Wideband Communications and Radar: Part II, UWB Radars and Sensors.” *Microwave Journal* (Feb. 2001), pp. 22–52.

[108] O’Meara, T. R. “The synthesis of band-pass, all-pass time delay networks with graphical approximation techniques.” *Research Rept. 114* (1959).

[109] Hoffswell, R. A. “A Microstrip Line Stretcher.” *Review of Scientific Instruments* 41.9 (Nov. 2003), pp. 1330–1331. DOI: 10.1063/1.1684808.

[110] Caputi, W. J. “Stretch: A Time-Transformation Technique.” *IEEE Transactions on Aerospace and Electronic Systems* AES-7.2 (1971), pp. 269–278. DOI: 10.1109/TAES.1971.310366.

[111] Ishii, M., Yamada, G., and Miyatake, H. “US Patent No. US20130141148A1, Pulse stretching circuit and method.” 2011. URL: https://patents.google.com/patent/US20130141148A1/en.

[112] Xiang, B. et al. “An integrated Ku-band nanosecond time-stretching system using improved dispersive delay line (DDL).” *2012 IEEE 12th Topical Meeting on Silicon Monolithic Integrated Circuits in RF Systems*. 2012, pp. 151–154. DOI: 10.1109/SiRF.2012.6160140.

[113] Zverev, A. I. *Handbook of Filter Synthesis*. John Wiley and Sons, Inc., 1967.

[114] Monti, G., and Tarricone, L. “Negative Group Velocity in a Split Ring Resonator-Coupled Microstrip Line.” *Progress In Electromagnetics Research* 94 (2009), pp. 33–47. DOI: 10.2528/PIER09052801.

[115] Regalia, P., Mitra, S., and Vaidyanathan, P. “The digital all-pass filter: a versatile signal processing building block.” *Proceedings of the IEEE* 76.1 (1988), pp. 19–37. DOI: 10.1109/5.3286.

[116] Caloz, C. et al. “Analog Signal Processing: A Possible Alternative or Complement to Dominantly Digital Radio Schemes.” *IEEE Microwave Magazine* 14.6 (2013), pp. 87–103. DOI: 10.1109/MMM.2013.2269862.

[117] Elamien, M. B. et al. “Synthesis of Wideband High-Quality Factor Delay- Tunable Fully Differential All-Pass Filters.” *IEEE Transactions on Microwave Theory and Techniques* 68.10 (2020), pp. 4348–4360. DOI: 10.1109/TMTT.2020.3011723.

[118] França Ferreira, J. A. de et al. “Design and Synthesis of Arbitrary Group Delay Filters for Integrated Analog Signal Processing.” *2018 25th IEEE International Conference on Electronics, Circuits and Systems (ICECS)*. 2018, pp. 613–616. DOI: 10.1109/ICECS.2018.8617912.

[119] Zhang, Q., Gupta, S., and Caloz, C. “Synthesis of Narrowband Reflection-Type Phasers With Arbitrary Prescribed Group Delay.” *IEEE Transactions on Microwave Theory and Techniques* 60.8 (2012), pp. 2394–2402. DOI: 10.1109/TMTT.2012.2198486.

[120] Zhang, Q., Sounas, D. L., and Caloz, C. “Synthesis of Cross-Coupled Reduced-Order Dispersive Delay Structures (DDSs) With Arbitrary Group Delay and Controlled Magnitude.” *IEEE Transactions on Microwave Theory and Techniques* 61.3 (2013), pp. 1043–1052. DOI: 10.1109/TMTT.2013.2241785.

[121] Gupta, S. et al. “Group-Delay Engineered Noncommensurate Transmission Line All-Pass Network for Analog Signal Processing.” *IEEE Transactions on Microwave Theory and Techniques* 58.9 (2010), pp. 2392–2407. DOI: 10.1109/TMTT.2010.2058933.

[122] Avignon-Meseldzija, E., Anastasov, J., and Milic, D. “A linear group delay filter with tunable positive slope for analog signal processing.” *International Journal of Circuit Theory and Applications* 49.5 (2021), pp. 1307–1326. DOI: https://doi.org/10.1002/cta.2995.

[123] Mondal, I., and Krishnapura, N. “Expansion and Compression of Analog Pulses by Bandwidth Scaling of Continuous-Time Filters.” *IEEE Transactions on Circuits and Systems I: Regular Papers* 65.9 (2018), pp. 2703–2714. DOI: 10.1109/TCSI.2018.2799080.

[124] Pactitis, S. A. *Active Filters: Theory and Design*. CRC Press, 2007.

[125] Rauscher, C. “Microwave Active Filters Based on Transversal and Recursive Principles.” *IEEE Transactions on Microwave Theory and Techniques* 33.12 (1985), pp. 1350–1360. DOI: 10.1109/TMTT.1985.1133225.

[126] Xia, J., Law, C. L., and Jiang, J. “A Novel 3–5 GHz Active Matched Filter for Impulse Radio Ultra-Wideband.” *IEEE Microwave and Wireless Components Letters* 19.7 (2009), pp. 458–460. DOI: 10.1109/LMWC.2009.2022133.

[127] Jarjar, M., and Ouazzani, N. P. el. “Three branch microwave channelized active bandpass filter.” *2019 International Conference on Wireless Networks and Mobile Communications (WINCOM)*. 2019, pp. 1–5. DOI: 10.1109/WINCOM47513.2019.8942576.

[128] Gomez-Garcia, R. et al. “Flexible Filters: Reconfigurable-Bandwidth Bandpass Planar Filters with Ultralarge Tuning Ratio.” *IEEE Microwave Magazine* 15.5 (2014), pp. 43–54. DOI: 10.1109/MMM.2014.2321094.

[129] Thomson, W. “Delay networks having maximally flat frequency characteristics.” English. *Proceedings of the IEE - Part III: Radio and Communication Engineering* 96 (44 Nov. 1949), 487–490(3). ISSN: 0369-8947. URL: https://digital-library.theiet.org/content/journals/10.1049/pi-3.1949.0101.

[130] Mini-circuits. *Low Pass Filter SLP-2400+*. URL: https://www.minicircuits.com/pdfs/SLP-2400+.pdf.

[131] Paschotta, R. *Pulse Stretchers*. URL: https://www.rp-photonics.com/pulse_stretchers.html.

[132] Steed, R. *Modelling of Optical Pulse Stretching using Circulating Cavities*. Feb. 2015. DOI: 10.13140/2.1.3310.4169.

[133] Ulyanov, I., Przhiialkovskii, D. V., and Butov, O. V. “Point-by-point inscription of chirped apodized fiber Bragg gratings for application as ultrashort pulse stretchers.” *Results in Physics* 32 (2022), p. 105101. ISSN: 2211-3797. DOI: https://doi.org/10.1016/j.rinp.2021.105101.

[134] Williamson, A. P., and Kiefer, J. “Polarization-controlled optical ring cavity (PORC) tunable pulse stretcher.” *Optics Communications* 372 (2016), pp. 98–105. ISSN: 0030-4018. DOI: https://doi.org/10.1016/j.optcom.2016.03.091.

[135] Saraceno, C. “Pulse stretching and compressing using grating pairs.” *Photonics and Ultrafast Laser Science*. Ibsen Photonics A/S, 2017, pp. 1–8. URL: https://ibsen.com/wp-content/uploads/White-paper-Pulse-stretching-and-compressing-using-grating-pairs_v1.pdf.

[136] Lim, C. et al. “Evolution of Radio-Over-Fiber Technology.” *Journal of Lightwave Technology* 37.6 (2019), pp. 1647–1656. DOI: 10.1109/JLT.2018.2876722.

[137] Beas, J. et al. “Millimeter-Wave Frequency Radio over Fiber Systems: A Survey.” *IEEE Communications Surveys &amp Tutorials* PP (Mar. 2013), pp. 1–27. DOI: 10.1109/SURV.2013.013013.00135.

[138] ITU-R. *Report ITU-R M.2516-0: Future technology trends of terrestrial International Mobile Telecommunications systems towards 2030 and beyond*. Nov. 2022.

[139] Wikström, G. et al. “Challenges and Technologies for 6G.” *2020 2nd 6G Wireless Summit (6G SUMMIT)*. 2020, pp. 1–5. DOI: 10.1109/6GSUMMIT49458.2020.9083880.

[140] Puerta, R. et al. “Analog Mobile Fronthaul for 6G and Beyond.” *Journal of Lightwave Technology* (2024), pp. 7458–7467. DOI: 10.1109/JLT.2024.3435770.

[141] Podbregar, L. et al. “Advances in and Applications of Microwave Photonics in Radar Systems: A Review.” *Photonics* 12.6 (2025). ISSN: 2304-6732. DOI: 10.3390/photonics12060529.

[142] Nakamura, K. et al. “Verification of Applicability of 90 GHz Band Millimeter-Wave for Obstacle Detection to Railway.” *IEEJ Transactions on Electrical and Electronic Engineering* 18.6 (2022), pp. 960–969. DOI: https://doi.org/10.1002/tee.23766.

[143] Kohmura, A. et al. “Optical fiber connected millimeter-wave radar for FOD detection on runway.” *2013 European Radar Conference*. 2013, pp. 41–44.

[144] Kawanishi, T. et al. “Optical fiber network-connected distributed mm-wave radar system.” *2017 IEEE Photonics Society Summer Topical Meeting Series (SUM)*. 2017, pp. 197–198. DOI: 10.1109/PHOSST.2017.8012718.

[145] Ostrovskis, A. et al. “Experimental Demonstration of Hybrid Photonics-BasedARoF System for 5G and B5G Networks.” *2022 International Conference on Software, Telecommunications and Computer Networks (SoftCOM)*. 2022, pp. 1–5. DOI: 10.23919/SoftCOM55329.2022.9911478.

[146] Jiang, W., and Schotten, H. D. “Full-Spectrum Wireless Communications for 6G and Beyond: From Microwave, Millimeter-Wave, Terahertz to Lightwave.” *2023 IEEE 3rd International Conference on Computer Communication and Artificial Intelligence (CCAI)*. 2023, pp. 353–357. DOI: 10.1109/CCAI57533.2023.10201316.

[147] Li, W. et al. “Over 100 Gb/s mm-wave delivery with 4600 m wireless distance based on dual polarization multiplexing.” *Science China Information Sciences* 66.224301 (2023), pp. 1869–1919. DOI: 10.1007/s11432-023-3834-5.

[148] Jia, S. et al. “Integrated Dual-Laser Photonic Chip for High-Purity Carrier Generation Enabling Ultrafast Terahertz Wireless Communications.” *Nature Communications* 13.1 (Mar. 2022), p. 1388. ISSN: 2041-1723. DOI: 10.1038/s41467-022-29049-2.

[149] Jiang, T. et al. “Photonics-Enabled 6G Distributed MIMO: Experimental Study in an Indoor Environment.” *2024 International Topical Meeting on Microwave Photonics (MWP)*. 2024, pp. 1–5. DOI: 10.1109/MWP62612.2024.10736285.

[150] Anes, B., and Riad, B. A. “A new bidirectional analog radio over fiber transmission for 5G millimeter wave communication systems.” *2022 International Conference of Advanced Technology in Electronic and Electrical Engineering (ICATEEE)*. 2022, pp. 1–6. DOI: 10.1109/ICATEEE57445.2022.10093741.

[151] Perez-Galacho, D., Sartiano, D., and Sales, S. “Analog Radio over Fiber Links for Future 5G Radio Access Networks.” *2019 21st International Conference on Transparent Optical Networks (ICTON)*. 2019, pp. 1–4. DOI: 10.1109/ICTON.2019.8840516.

[152] Delmade, A. et al. “Expanded Gain-Switched Comb Source for 180 – 260 GHz Sub-THz Analog Radio-over-Fiber 6G Wireless System.” *2024 Optical Fiber Communications Conference and Exhibition (OFC)*. 2024, pp. 1–3.

[153] de Souza Lopes, C. H., Saia Lima, E., and Sodré Junior, A. C. “RoF/FSO-based Fronthaul for 5G Systems and Beyond.” *2021 SBMO/IEEE MTT-S International Microwave and Optoelectronics Conference (IMOC)*. Oct. 2021, pp. 1–3. DOI: 10.1109/IMOC53012.2021.9624921.

[154] Yao, J. “Microwave Photonics.” *Journal of Lightwave Technology* 27.3 (Feb. 2009), pp. 314–335. ISSN: 1558-2213. DOI: 10.1109/JLT.2008.2009551.

[155] Nguyen, D.-N. et al. “Optical Hybrid Fiber/Free-Space and 25 GHz Wireless Transmission Using LTE M-QAM Signals.” *2019 22nd International Symposium on Wireless Personal Multimedia Communications (WPMC)*. Nov. 2019, pp. 1–6. DOI: 10.1109/WPMC48795.2019.9096169.

[156] Azizpour, R. et al. “Multi-Channel Radio-Over-Fiber Communication Systems Through Modulation Instability Phenomenon.” *IEEE Photonics Journal* 16.5 (2024), pp. 1–13. DOI: 10.1109/JPHOT.2024.3446314.

[157] Jia, Z., Yu, J., and Chang, G.-K. “A Full-Duplex Radio-over-Fiber System Based on Optical Carrier Suppression and Reuse.” *IEEE Photonics Technology Letters* 18.16 (Aug. 2006), pp. 1726–1728. ISSN: 1941-0174. DOI: 10.1109/LPT.2006.879946.

[158] Eventech LTD. *ESTT 7 Series*. URL: https://eventechsite.com/products/%5C#estt7series.

[159] Srivastav, A., and Mandal, S. "Radars for Autonomous Driving: A Review of Deep Learning Methods and Challenges." *IEEE Access* 11 (2023), pp. 97147–97168. DOI: 10.1109/ACCESS.2023.3312382.

[160] Enayati, J., Asef, P., and Wilson, P. "Resilient Multi-Range Radar Detection System for Autonomous Vehicles – A New Statistical Method." *Journal of Electrical Engineering and Technology* 19 (May 2023), p. 15. DOI: 10.1007/s42835-023-01567-z.

[161] Ruiz-Carregal, G. et al. "Ku-Band SAR-Drone System and Methodology for Repeat-Pass Interferometry." *Remote Sensing* 16.21 (2024). DOI: 10.3390/rs16214069.

[162] Nandana, V. et al. "Characterization of Drop Size Distribution in Urban Heavy Rainfall Event Using Doppler Weather Radar and Laser Precipitation Monitor." *Remote Sensing in Earth Systems Sciences* 9 (Nov. 2025). DOI: 10.1007/s41976-025-00251-2.

[163] Gini, F. "Grand Challenges in Radar Signal Processing." *Frontiers in Signal Processing* 1 (Mar. 2021). DOI: 10.3389/frsip.2021.664232.

[164] Yuksekkaya, F., Franchi, N., and Lubke, M. "On the Detection of Vulnerable Road Users—Simulating Limits of an FMCW Radar." *Electronics* 13 (June 2024), p. 2547. DOI: 10.3390/electronics13132547.

[165] Santacruz, J. P. et al. "Analysis and Compensation of Phase Noise in FMCW LiDAR Sensors." *J. Lightwave Technol.* 43.12 (June 2025), pp. 5636–5644.

[166] Bauduin, M., and Bourdoux, A. "Impact of Phase Noise on FMCW and PMCW Radars." *2023 IEEE Radar Conference (RadarConf23)*. 2023, pp. 1–6. DOI: 10.1109/RadarConf2351548.2023.10149598.

[167] Tschapek, P. et al. "Detailed Analysis and Modeling of Phase Noise and Systematic Phase Distortions in FMCW Radar Systems." *IEEE Journal of Microwaves* 2.4 (2022), pp. 648–659. DOI: 10.1109/JMW.2022.3195574.

[168] Liu, F. et al. "Seventy Years of Radar and Communications: The road from separation to integration." *IEEE Signal Processing Magazine* 40.5 (2023), pp. 106–121. DOI: 10.1109/MSP.2023.3272881.

[169] *Super High Frequency (SHF) Communication Market Report, Industry and Market Size & Revenue, Share, Forecast 2024–2030*. Published August 2025; Report ID: 12970351; Historical Data: 2017–2023. Strategic Market Research, 2025. URL: https://www.strategicmarketresearch.com/market-report/super-high-frequency-communication-market.

[170] Rieländer, D. et al. “ESA Ground Infrastructure for the NASA/JPL PSYCHE Deep-Space Optical Communication Demonstration.” *International Conference on Space Optics – ICSO 2022*. Ed. by Minoglou, K., Karafolas, N., and Cugny, B. Dubrovnik, Croatia: SPIE, July 2023, p. 13. DOI: 10.1117/12.2688805.

[171] Khatri, F. I. et al. “Space-to-Ground Optical Interface Verification for the Orion Artemis II Optical (O2O) Communications Demonstration.” *2023 IEEE International Conference on Space Optical Systems and Applications (ICSOS)*. Oct. 2023, pp. 26–30. DOI: 10.1109/ICSOS59710.2023.10491223.

[172] Chen, P. et al. “Range-Velocity Measurement Accuracy Improvement Based on Joint Spatiotemporal Characteristics of Multi-Input Multi-Output Radar.” *Remote Sensing* 16.14 (July 2024). ISSN: 2072-4292. DOI: 10.3390/rs16142648.

[173] Jacobs, L. et al. “On the Accuracy of Automotive Radar Tracking.” *2023 IEEE 97th Vehicular Technology Conference (VTC2023-Spring)*. June 2023, pp. 1–6. DOI: 10.1109/VTC2023-Spring57618.2023.10200523.

[174] Singh, P. et al. “Comprehensive Survey on Radar Systems and Its Target Classification Techniques.” *Journal of Electronics and Electrical Engineering* (Feb. 2025), pp. 234–269. ISSN: 2972-3280. DOI: 10.37256/jeee.4120255934.

[175] Blanche, P.-A. et al. “A 300 THz Tabletop Radar Range System with Sub-Micron Distance Accuracy.” *Scientific Reports* 8.1 (Sept. 2018), p. 14443. ISSN: 2045-2322. DOI: 10.1038/s41598-018-32846-9.



Sandis Migla was born in 1999 in Riga. He earned a Bachelor's degree in Electrical Science (2021) and a Master's degree in Electronics and the Qualification of Lead Electronics Engineer (2023) from Riga Technical University. Since 2020, he has worked at Riga Technical University, currently holding the positions of researcher and lecturer. His research interests include integrated sensing and communications, space communications, and radar systems.